In presenting the dissertation as a partial fulfillment of the requirements for an advanced degree from the Georgia Institute of Technology, I agree that the Library of the Institute shall make it available for inspection and circulation in accordance with its regulations governing materials of this type. I agree that permission to copy from, or to publish from, this dissertation may be granted by the professor under whose direction it was written, or, in his absence, by the Dean of the Graduate Division when such copying or publication is solely for scholarly purposes and does not involve potential financial gain. It is understood that any copying from, or publication of, this dissertation which involves potential financial gain will not be allowed without written permission.

7/25/68

INFLUENCE OF LOAD PERTURBATIONS ON THE TIME-RESPONSE OF AN INCREMENTAL DIGITAL FEEDBACK NUMERICAL CONTROL MACHINE TOOL

A THESIS

Presented to

The Faculty of the Division of Graduate

Studies and Research

by

Jean-Louis Suzan

In Partial Fulfillment

of the Requirements for the Degree

Master of Science in Mechanical Engineering

Georgia Institute of Technology

December, 1971

INFLUENCE OF LOAD PERTURBATIONS ON THE TIME-RESPONSE OF AN INCREMENTAL DIGITAL FEEDBACK NUMERICAL CONTROL MACHINE TOOL

Approved:

Chairman

Date approved by Chairman: Nov. 10, 1971

ACKNOWLEDGEMENTS

My deepest appreciation and respect are expressed to Dr. Albert L. Holliman, who has unfailingly provided sound advice, knowledgeable guidance, and cheerful encouragement to me during the conduct of this research.

Special acknowledgement is also due to Dr. S. L. Dickerson who, as a member of my thesis advisory committee and instructor of a sequence of three graduate courses in control theory, has provided the fundamental guidance to my studies in the School of Mechanical Engineering.

Dr. John B. Peatman is due a special note of thanks for his sincere interest and constructive comments as reader.

Finally, I am indebted to Mrs. Claudine Taylor for her assistance in typing the manuscript, to William H. Tucker and Michel L. P. Camerman for their assistance in the drawing of the figures.

TABLE OF CONTENTS

TABLE OF CONTENTS (CONTINUED)

LIST OF ILLUSTRATIONS

LIST OF ILLUSTRATIONS (CONTINUED)

LIST OF ILLUSTRATIONS (CONCLUDED)

SUMMARY

This work is mainly concerned with the mathematical modeling of the various components of a classical machine tool operated with an incremental digital feedback control system.

The analysis of such a system presents challenging problems in the areas of mechanical engineering, electronics, and hydraulics. Two chapters are devoted to the modeling of the electromechanical and electrohydraulic elements, while two others are devoted to the numerical control system and its necessary associated compensation devices. The modeling of the mechanical transmissions is conducted in great detail. Chapter VI and conclusions are the formulation of further studies.

Each of the major machine components is studied separately and a model using a block diagram representation is developed, keeping in mind the possibility of a further simulation on an analog computer. Special care is taken to allow the understanding of the interconnection, in the total system, of the feedback loops describing every single component. Thus, a machine tool becomes a multiple feedback loop control system.

Particular attention is given to the identification of the major load sources, whether they are outside or within the total system control loop.

CHAPTER I

INTRODUCTION

The Control Problem

Some machine tools, such as large portal milling machines, may have a total weight over 200,000 lbs with moving elements reaching 120,000 lbs and requiring accelerations of as much as 50 in per sec^2. The servodrives of these machines must control the velocity of the slides, or the feed rates, throughout a range from 0.25 inch per minute up to 100 inches per minute (1). A slight variation in the velocity, or feed rate, can deteriorate the surface finish of the workpiece whose specifications are less than 100 microinches. The servodrives must also control the position of the moving elements of a machine tool within an error limit of a few thousandths of an inch.

Thus, the control problem becomes that of accurately and continuously controlling the position of the moving elements, in response to a prepared reference input, in the presence of various types of load disturbances.

If the performance of the controlled part of the process is to be predicted with any degree of accuracy, then it is necessary to fully understand the operation of the individual elements, within the control loop, and to detect the load disturbances which affect the system behaviour.

Literature Survey

The current literature is rich in references about modern control theory (2), (3). Unfortunately, most of the studies are theoretical and far from the applied problems of a machine tool designer who too often ignores the control aspect of his equipment and merely concentrates his research work on purely mechanical questions such as strength of materials, power transmission, friction, etc. By chance, sometimes, vibration analysis and its associated differential equations make him use the current language of the control engineer.

However, literature is not abundant in papers describing a numerical control machine tool as a complex system composed of numerous interacting loops (1); one is more likely to find fractional analysis either of the digital circuits (4) or of the hydraulic components (5) or of the structure (6). The Cincinnati Milling Machine Company (1), in the U.S.A., and the Machine Tool Design and Research Conference (7), in Great Britain, are involved in some research programs whose objective is to improve machine tool design using Modern Control Theory.

Purpose of the Research

The study of a numerical control machine tool presents unique challenging problems in the area of mechanical design, electronics, and hydraulics. The successful marriage of the elements, in these three fields, should be the result of a synthesis made by means of modern control theory.

To allow such a synthesis, a classical milling machine structure has been selected, as shown in Figure 1.

Using linear and nonlinear control theory, the study will investigate the following groups of elements composing a schematized numerical control machine tool.

1. electro-mechanical components such as gears, transmission screws, guide-ways and bed structure.
2. hydraulic actuator, a fixed displacement axial piston rotary motor.
3. electro-hydraulic servovalve, a two-stage type.
4. numerical control equipment such as a bidirectional counter, a digital-analog converter, a position feedback quantizer and other electronic elements composing compensation loops.
5. electric motor, the rotary actuator of the spindle and cutter.

Special care will be devoted to the identification of the load perturbation sources and particularly to the effects generated by the metal cutting process.

Figure 2 represents a simplified block diagram for the schematized numerical control machine tool of Figure 1. For clarity, at this stage of the study, load disturbances have been limited to the cutting effort, while a single transfer function characterizes the behaviour of all the mechanical components of the machine; some other feedback compensation loops will be added further in the study.

The main objective of this study is to provide the N/C machine tool designer and user with a synthetic model taking into account the fundamental components of the system and the load perturbations induced during the metal cutting process. This model might contribute to the detection of the causes of an undesirable

response pattern such as a "staircase" shaped time response, an unstable behaviour, a large position or velocity error, under or overdamped characteristics, etc.

The first chapters are devoted to the modeling while Chapters VI and VII (Conclusions) give suggestions for further research such as the simulation on an analog computer and the stability analysis required by the presence of nonlinearities.

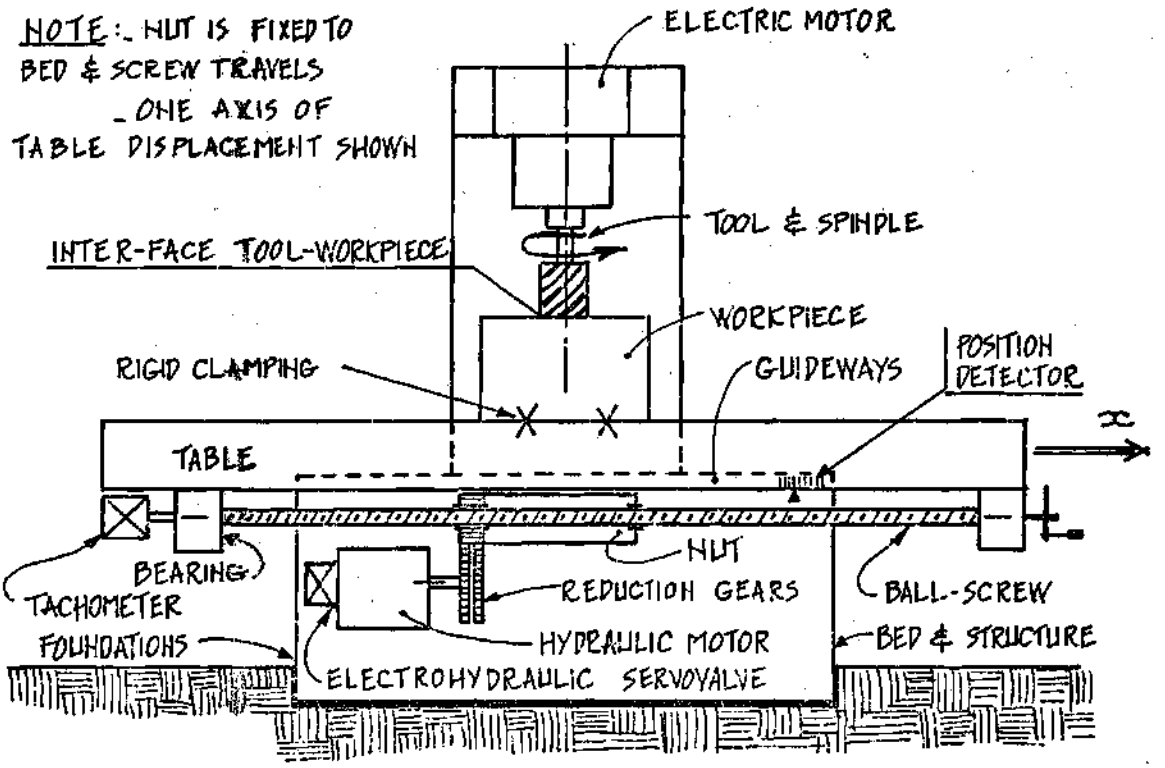

Figure 1. A Schematized N/C Machine Tool.

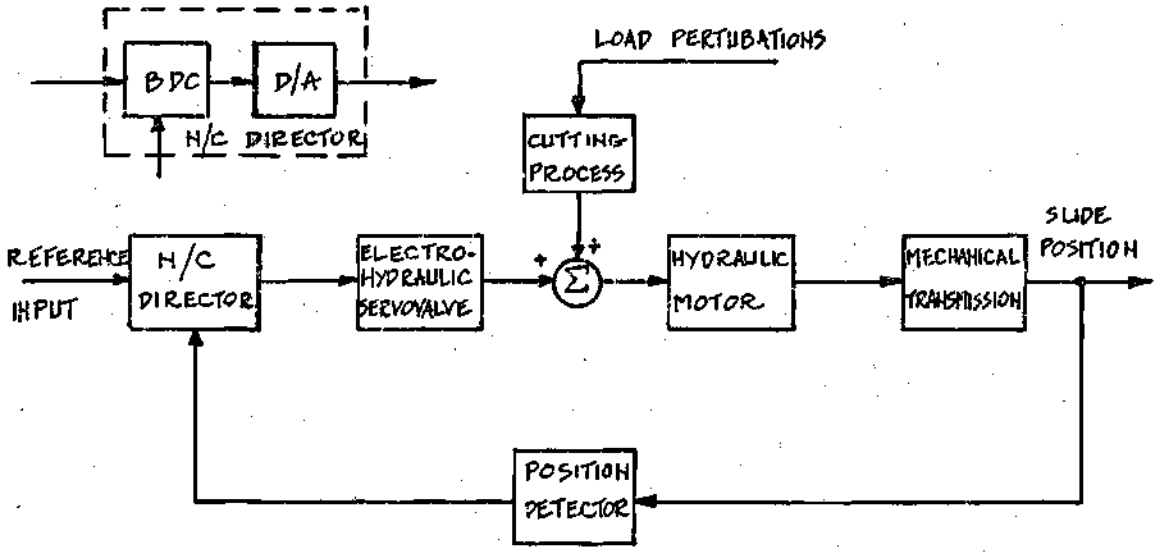

Figure 2. Simplified Model of a N/C Machine Tool.

CHAPTER II

MODELING OF THE ELECTRO-MECHANICAL COMPONENTS

The Metal Cutting Process

Milling Process on a Single Degree of Freedom System

As shown in Figure 1, only one direction of displacement is considered for the machine table. It is assumed that the only vibration direction, the resultant cutting force and the table displacement along the horizontal x-direction are parallel and contained in the same vertical plane.

A model of the cutting process to be investigated is shown in Figure 3. The resultant cutting force, F_x, is applied to the middle of the arc of contact between the tool and the workpiece and its direction is normal to the cut surface. The instantaneous cutting force, F_i, acting at a single tooth of the cutter is due to the dynamic chip thickness variation, u. Its direction is defined by the angles φ_i and β, where φ_i characterizes the instantaneous position of the tooth and β the angle between F_i and the radial direction. The subscript "i" is used to identify any particular tooth. As shown in Figure 4, the maximum chip thickness occurs in the radial direction. With this notation, the cutting force component, caused by the table displacement, in the x-direction is formulated as follows:

$$F_{ix} = k_1 \cdot u_x \cdot \sin\varphi_i \sin(\varphi_i + \beta)$$

where k_1 is a coefficient and u_x is defined by

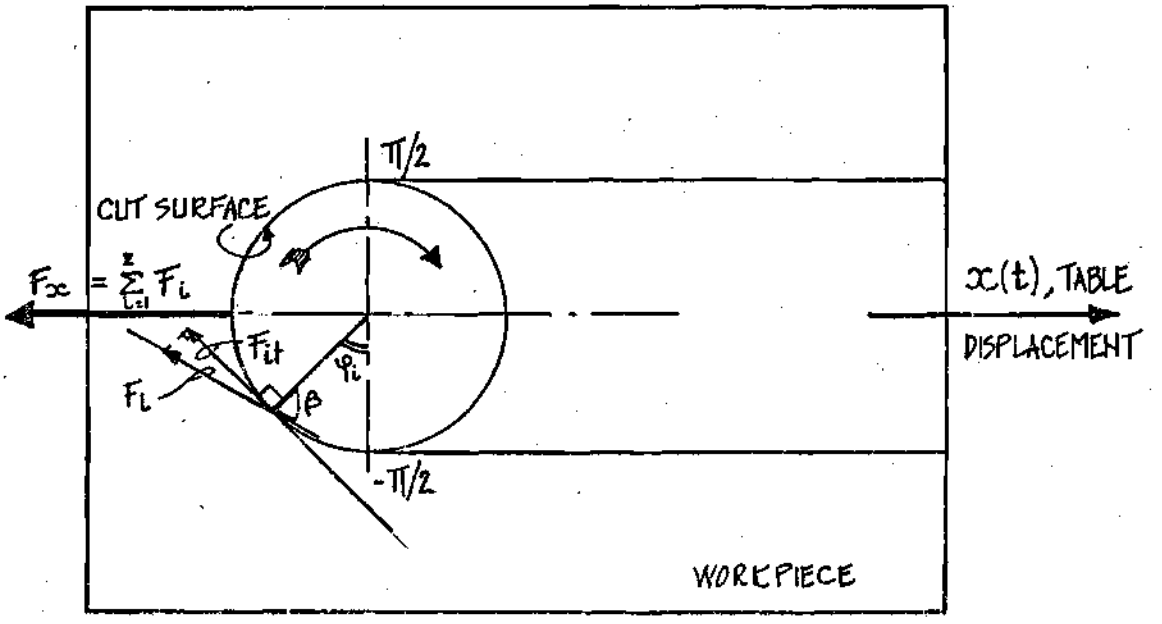

Figure 3. Model of the Cutting Process.

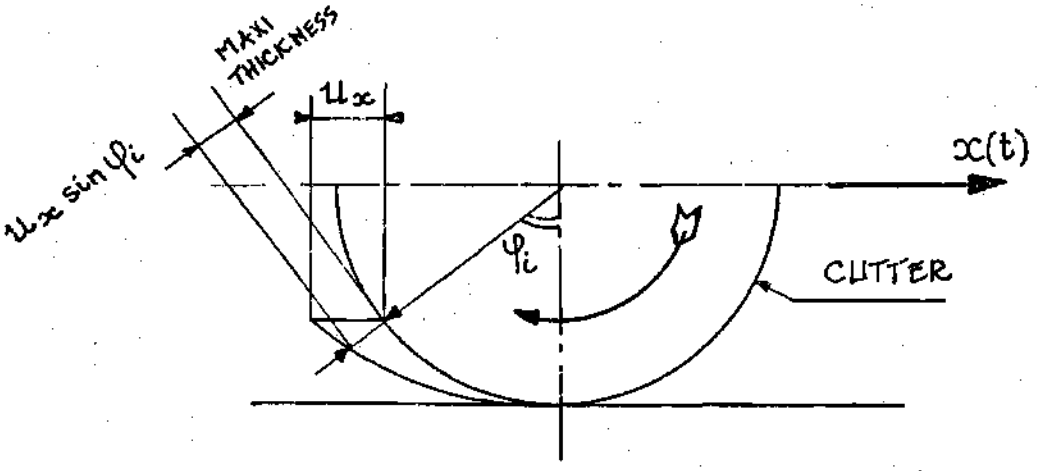

Figure 4. Chip Formation.

$$u_x = x\left(t - \frac{T}{z}\right) - x(t)$$

with T, the period of rotation for the cutter and z, the number of teeth of the cutter.

The product of the two circular functions

$$R_i = \sin \varphi_i \sin(\varphi_i + \beta)$$

is a time dependent coefficient since the position of the different teeth is continuously changing. As several blades of the cutter are milling simultaneously, the total force F_x applied in the x-direction is given by the summation of the components acting at the different teeth in contact with the cut surface.

$$F_x = \sum_{i=1}^{z} F_{ix} = k_1\left[x(t - \frac{T}{z}) - x(t)\right] \cdot \sum_{i=1}^{z} R_i \qquad (1)$$

where

$$R_i = R_i(\varphi_i) \quad \text{for} \quad \varphi_1 + 2n\pi \leq \varphi_i \leq \varphi_2 + 2n\pi$$

$$R_i = 0 \quad \text{for} \quad \varphi_2 + 2n\pi \leq \varphi_i \leq \varphi_1 + 2n\pi$$

with φ_1 indicating the angle value for which a tooth begins to cut and φ_2 the angle value for which the tooth stops to cut.

In order to simplify the computation of the total cutting effort, F_x, the present problem with a time varying coefficient can be reduced to a system with a time invariant coefficient. The coefficient R_i can be approximated by its time average. Thus it comes

$$F_x = k_1 u_x \frac{z_c}{\varphi_2 - \varphi_1} \int_{\varphi_1}^{\varphi_2} \sin\varphi \sin(\varphi+\beta)\, d\varphi$$

with z_c the number of teeth in contact with the cut surface.

A simplified form is given by

$$F_x = K\left[x\left(t - \frac{1}{zf}\right) - x(t)\right] \qquad (2)$$

where k is a constant and f the frequency of rotation for the cutter.

Numerical Application. Lets assume

$$\varphi_1 = -90^o$$

$$\varphi_2 = +90^o$$

$$\beta = 60^o$$

$$z = 10$$

$$z_c = 5$$

this gives

$$F_x = \frac{5}{4} k_1 \left[x\left(t - \frac{1}{zf}\right) - x(t)\right]$$

Load Torque Acting on the Spindle and Cutter

The projection of F_i on the tangent to the cut surface at the contact between the blade and the cut surface, F_{it}, is needed to evaluate the load torque T_L to which the spindle and cutter are submitted. It comes

$$F_{it} = k_1 u_x \sin\varphi_i \cos\left(\frac{\pi}{2} - \beta\right)$$

The Load Torque, T_L, is given by the expression

$$T_L = \frac{d}{2} k_1 u_x \cos\left(\frac{\pi}{2} - \beta\right) \sum_{i=1}^{z} R_i' \qquad (3)$$

with

$$R_i' = \sin \varphi_i \quad \text{for } \varphi_1 + 2n\pi \leq \varphi_i \leq \varphi_2 + 2n\pi$$

$$R_i' = 0 \qquad \text{for } \varphi_2 + 2n\pi \leq \varphi_i \leq \varphi_1 + 2n\pi$$

and d, the diameter of the cutter.

As in the preceding paragraph, the time dependent coefficient, R_i', can be replaced by its time average, thus the following approximate expression can be written

$$T_L = k_1 u_x \cos\left(\frac{\pi}{2} - \beta\right) \frac{z_c}{\varphi_2 - \varphi_1} \int_{\varphi_1}^{\varphi_2} \sin\varphi \, d\varphi$$

a simplified form is

$$T_L = K'\left[x\left(t - \frac{1}{zf}\right) - x(t)\right] \qquad (4)$$

where K′ is a constant.

Numerical Application. Lets assume the same values as employed in the preceding paragraph. This gives

$$T_L = 2.76\left[x\left(t - \frac{1}{zf}\right) - x(t)\right]$$

The Rotary D.C. Actuator of the Cutter

General Equations

Following the trend of industry a classical D.C. motor with armature control has been selected. As the current literature provides many studies about the D.C. motor, Figure 5 and the following equations are sufficient to describe the operation of such an actuator.

$$T = K_T i_m$$

$$e_m = K_b \dot{\theta}_m$$

where $\dot{\theta}_m$ is the speed of rotation of the shaft, T the torque produced by the motor, i_m its armature current, e_m the back emf, K_T and K_b two constants. Thus the voltage equation is

$$L_m \frac{di_m}{dt} + R_m i_m + e_m = e_a$$

where L_m and R_m are the armature inductance and resistance and e_a the adjustable voltage applied to the armature. The torque equation at the motor shaft is

$$J\ddot{\theta}_m + B\dot{\theta}_m + T_L = T \qquad (5)$$

where J is the inertia load, B a damping coefficient and T_L an arbitrary load torque applied to the motor shaft.

Influence of Reduction Gears on a Rotary Actuator

A typical system is shown in Figure 6. The following equations can be

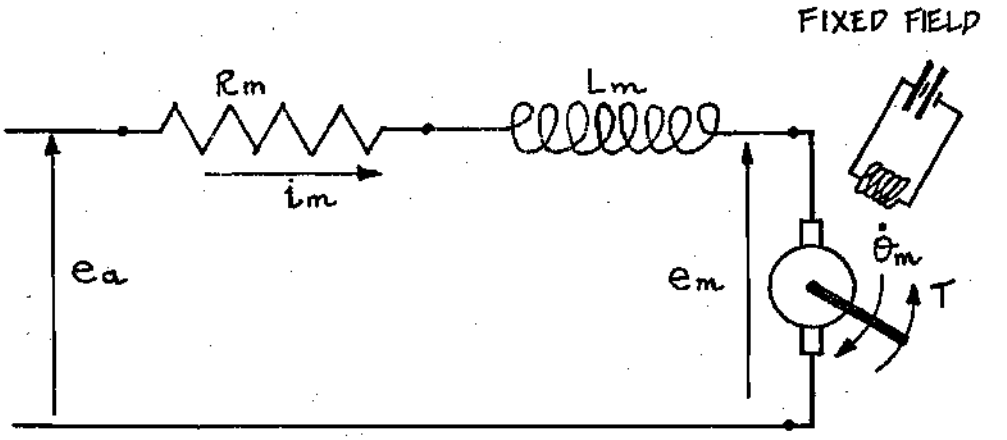

Figure 5. The D. C. Motor.

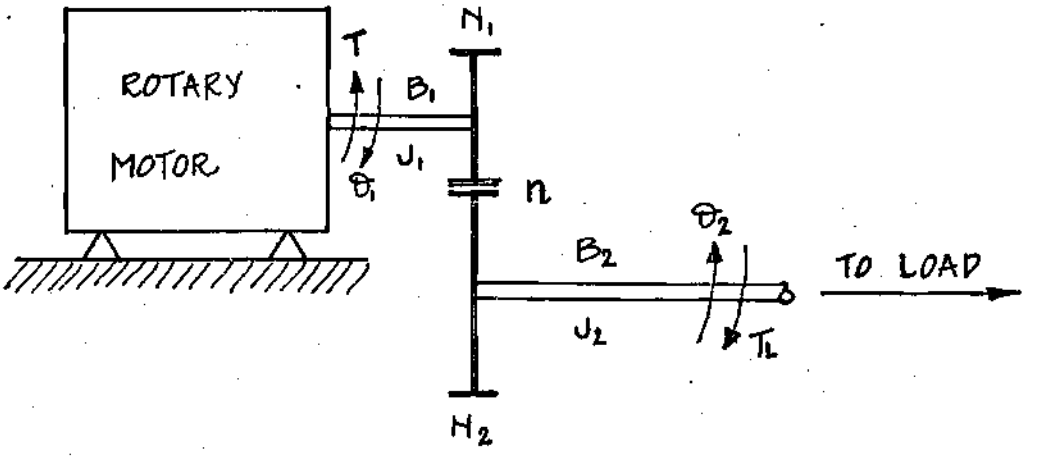

Figure 6. Reduction Gears.

written

$$J_1\ddot{\theta}_1 + B_1\dot{\theta}_1 + T_1 = T$$

$$J_2\ddot{\theta}_2 + B_2\dot{\theta}_2 + T_L = T_2$$

$$T_2 = nT_1$$

$$\theta_2 = \frac{\theta_1}{n}$$

where n is the reduction ratio, T_1 the restraining torque produced on gear 1 by gear 2, T_2 the driving torque produced on gear 2 by gear 1, T_L an arbitrary load torque produced on gear 2, T the driving torque produced by the actuator on gear 1, J_1, J_2 and B_1, B_2 the moments of inertia and damping coefficients of gears 1 and 2. Thus, it can be written

$$\left(J_1 + \frac{J_2}{n^2}\right)\ddot{\theta}_1 + \left(B_1 + \frac{B_2}{n^2}\right)\dot{\theta}_1 + \frac{T_L}{n} = T \qquad (6)$$

the two expressions between brackets represent the moment of inertia and damping of an equivalent system having mechanical characteristics equal to

$$J_{eq} = J_1 + \frac{J_2}{n^2} \qquad (7\text{-a})$$

$$B_{eq} = B_1 + \frac{B_2}{n^2} \qquad (7\text{-b})$$

and only one single dependent variable θ_1. It has been assumed that the shaft on

which the gears are mounted are very short, so that their stiffness may be considered as infinite.

The Compliant Drive of the Machine Table

Some Practical Considerations

They are needed to model a real drive system. Figure 7 represents the type of drive investigated. The input to the system is θ_1, the hydraulic motor output, i.e. the shaft rotation. θ_2 is the angular displacement of the lead-screw at position 2, just after the reduction gears. θ_3 is the angular displacement of the lead-screw at position 3; the cross section through the screw, at position 3, defines a vertical plane containing the center of gravity of the table-workpiece assembly. The workpiece is assumed to be clamped on the surface of the table by a perfectly rigid device. The difference of angle, $\theta_2 - \theta_3$, represents the angular deflection of the screw between positions 2 and 3. This deflection is caused by the effort of torsion, T, and the effort of compression, F, to which the screw is submitted. These efforts are induced by the cutting process, the table displacement and the various frictions occurring in the transmission nut, the thrust bearings and the guideways of the table.

In the following it is assumed that the resultant of the efforts applied to the table (or the workpiece) induces a uniform axial loading of the lead screw. Even in the case of side loads applied to the table, or the workpiece, it is possible to assure a uniform axial loading of the screw, a method is suggested in Figure 8.

Most of the lead screw transmissions are of the ball-bearing type. The idea that there is less friction in rolling than in sliding is at the base of this

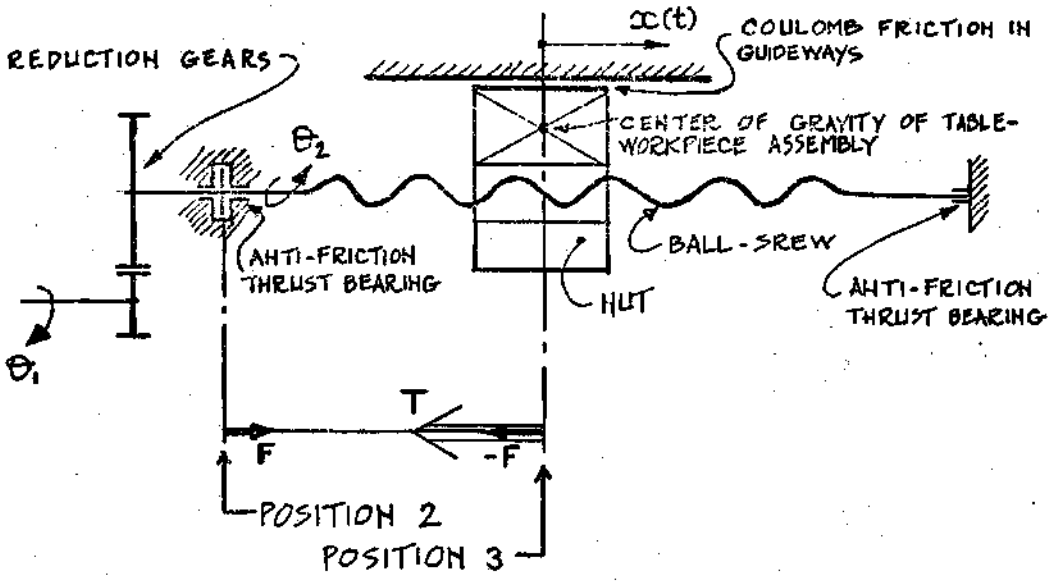

Figure 7. The Drive System.

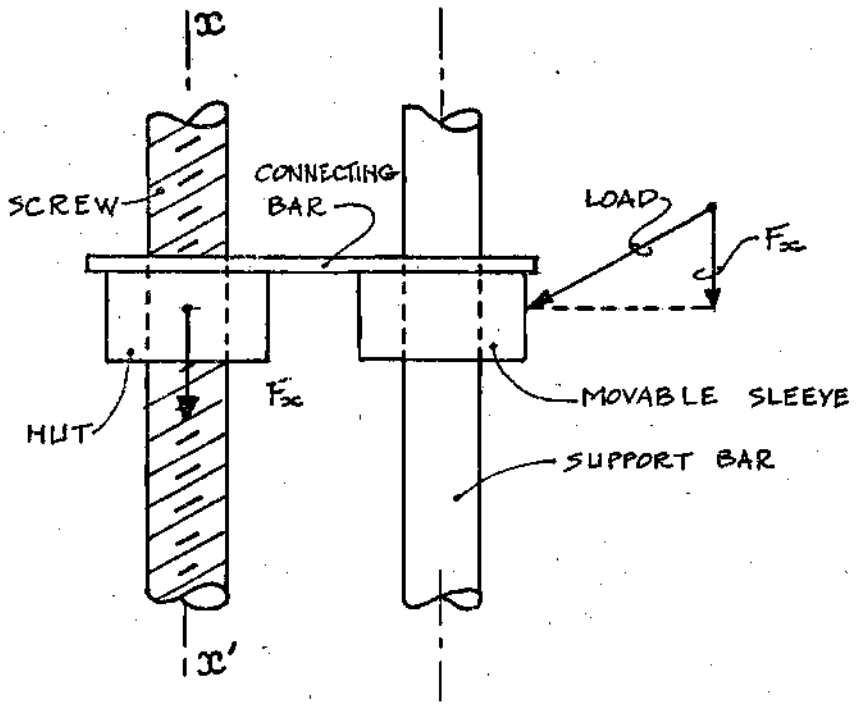

Figure 8. Method to Assure a Uniform Axial Loading at the Nut.

commonly used device. A typical ball-bearing screw is described as an assembly where "the screw and nut each have mating helical ball races; within the nut, the length of this race is filled with steel balls.... This construction thus forms a closed circuit through which the rolling balls,..., recirculate continuously as the screw and nut are rotated relative to each other" (8). As a result, friction losses are low and operating efficiencies run up to 98 per cent. In order to draw a maximum of benefit from this characteristic it is recommended that anti-friction bearings be used for the end-mounting of the lead screw.

A certain degree of backlash, due to the precision of the adjustment, is inevitable in ball bearing assemblies, this usually never exceeds 0.005 inch. The classical method of the anti-backlash gears is not advised with ball-bearing equipments, this would induce heavy friction losses and cut down the high efficiency of the system. The Saginaw Steering Gear Division, a General Motors Subsidiary, proposes a method to reduce the backlash; they employ two flange type nuts, mounted flange to flange, with a spacer between them, as shown in Figure 9; a precise adjustment of the end play is achieved by regulating the thickness of the spacer. A second type of friction appears when the lead screw starts to rotate, this is caused by a sliding motion between the balls and the race ways. If the backlash due to the precision of the ball-bearing assembly is small enough to be neglected but large enough to keep away from zero, it is possible to neglect the influence of this second non-linearity; the reason is that too small a backlash would cause a three-point contact between the balls and the race ways, as shown in Figure 10, and thus increase the starting friction effect. This simplification in

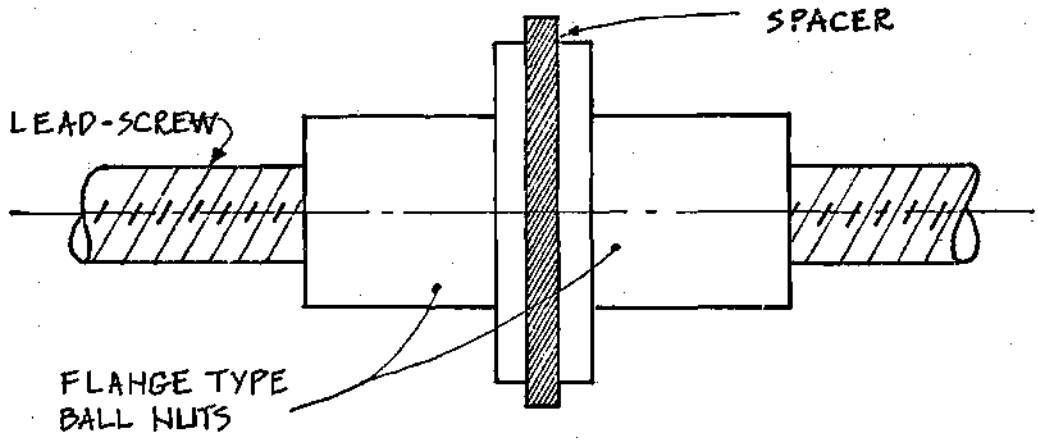

Figure 9. Elimination of Backlash.

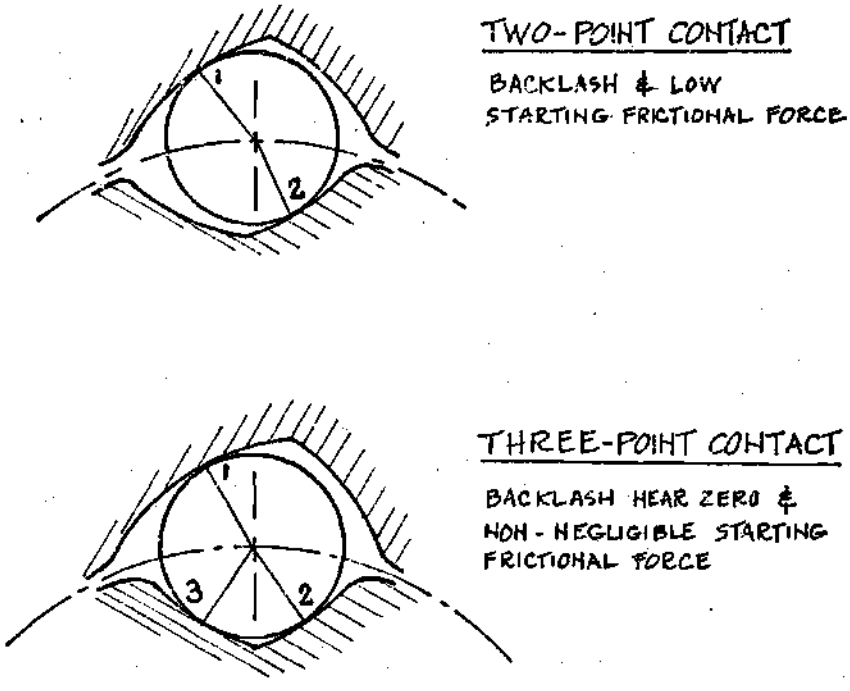

Figure 10. Backlash and Starting Friction Force.

the modeling process requires a satisfactory lubrication. A detailed analysis of the starting friction has been conducted by Z. Murase (8).

Because of the small magnitude of their friction losses, the ball-bearing transmissions must be equipped with no-back devices and braking systems in order to compensate the free-running action in either direction (9).

It is currently admitted that the friction in plain guideways, with metal-to-metal contact, is of the coulomb type. A closer analysis would include a static friction, also called striction, and a coulomb friction. This metal-to-metal contact is the cause of an unstable behaviour called "stick-slip," this might be avoided by the use of hydrostatic bearings whose main advantages are high load carrying capacity, high stiffness, the absence of metal-to-metal contact and their good damping characteristics (10).

A typical coulomb and striction friction is described by Figure 11. The friction in a system at rest is called static friction or striction. The frictional force F_s is equal to the force that is tending to produce motion as long as no motion actually occurs. As soon as the table starts to move, the friction force drops to F_c, the value of the coulomb friction which is not dependent upon the velocity except for its sign.

All these practical considerations allow the following assumptions for the modeling of a numerical control machine tool:

1. no significant backlash in the lead screw.
2. viscuous friction with a small damping coefficient for the screw and nut transmission.

3. no significant influence of the anti-friction thrust-bearings.

4. omission of the influence of the no-back and braking devices.

5. uniform axial loading of the lead screw.

6. coulomb friction in the slideways.

The Lead Screw Deflections

Appendix A describes a method to obtain a rough estimate for the axial stiffness, K_A, and the torsional stiffness, K_T, of the lead screw. Using the notation of Figure 7, it appears that the linear relation between the angular displacement of the screw and the linear displacement of the center of gravity of the table and workpiece assembly is valid at only one position labelled No. 3. There, the relation

$$x = \frac{L}{2\pi} \theta_3 \tag{8}$$

can be written with x, the displacement of the center of gravity of the table and workpiece assembly, and L, the lead of the thread of the screw. It can be written that

$$\theta_3 = \theta_2 - \Delta_T\theta - \Delta_A\theta \tag{9}$$

where

$$\Delta_T\theta = \frac{T}{K_T}$$

is the angular deflection due to the torsion torque, T, and

$$\Delta_A\theta = \frac{F}{K_A} \cdot \frac{2\pi}{L}$$

is the angular deflection due to the compression strength, F.

The Torsion Torque T. It is the summation of

1. T_1, the torque due to the cutting effort.
2. T_2, the torque due to a viscuous friction in the screw and nut transmission.
3. T_3, the torque due to a nonlinear coulomb friction in the slideways.
4. T_4, the torque required to accelerate the screw.

The torque T_1 is computed from the elements shown in Figure 12. The uniform axial loading of the screw due to the cutting effort, F_x, is characterized by a uniform distribution of forces along the helical surface of contact between the threads of the screw and the threads of the nut. The easiest method to study the forces applied to the screw consists of using the equivalent definition of the problem shown in Figure 13. This is a mass sliding on a slope, the mass is the equivalent of the nut while the slope angle, φ, corresponds to the helix angle of the thread. Thus,

$$T_1 = \frac{d}{2} \cot \varphi \cdot F_x$$

where d is the pitch diameter of the screw.

With equation (2), it comes

$$T_1 = K_1 K \left[x\left(t - \frac{T}{zf}\right) - x(t) \right] \tag{10}$$

where K_1 is a constant given by

$$K_1 = \frac{d}{2} \cot \varphi$$

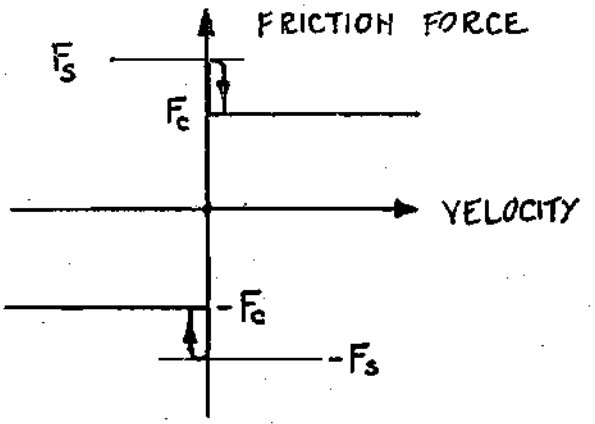

Figure 11. Typical Coulomb and Striction Frictions.

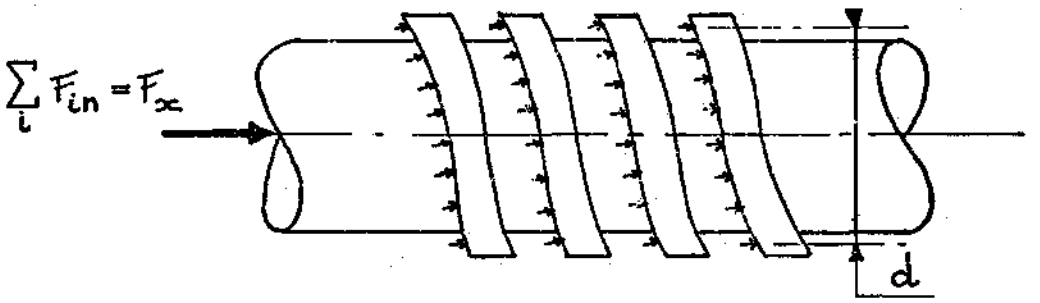

Figure 12. Uniform Axial Loading of the Screw.

$$\vec{F_x} = \vec{F_n} + \vec{F_t}$$

$$\begin{cases} F_t + F_n \cos\varphi = 0 \\ F_x + F_n \sin\varphi = 0 \end{cases}$$

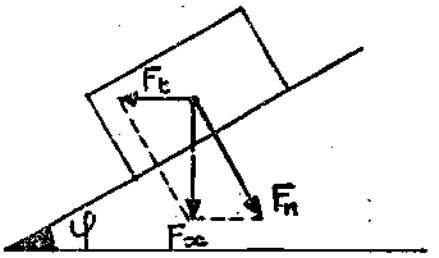

THUS $F_t = F_x \operatorname{cotg} \varphi$

Figure 13. Equivalent Problem.

A more accurate method could be developed to take into account the real shape of a ball bearing lead screw; in this case the rolling balls are the medium of force transfer.

A rough estimate of the viscuous friction torque, T_2, is obtained for a simplified type of lead screw defined in Figure 14. The viscuous friction force, F_v, is tangent to the surface of the thread and is oriented along the direction defined by the helix angle φ, as shown in Figure 15. The magnitude of F_v is proportional to the surface of the threads, A, and to the relative velocity of the thread of the screw with respect to the thread of the nut, v.

Thus

$$F_v = KAv = KA \frac{L\dot{\theta}_3}{2\pi \sin\varphi} \tag{11}$$

with L, the thread lead and $\dot{\theta}_3$, the velocity of the angular displacement of the screw at position 3, i.e. at the position generated by the vertical plane, normal to the screw-axis, containing the center of gravity of the table-workpiece assembly, recall Figure 7.

The tangential component of F_v is

$$F_t = \frac{KAL}{2\pi} \cdot \dot{\theta}_3$$

thus the friction torque becomes

$$T_2 = \frac{KAL}{2\pi} \cdot \frac{d}{2} \cdot \dot{\theta}_3 = K_2 \dot{\theta}_3 \tag{12}$$

where K_2 is a constant and d, the pitch diameter of the screw. The surface of the threads in contact is roughly

$$A = a \cdot \frac{\ell}{L} \cdot \pi d$$

with ℓ, the length of the threaded portion of the nut.

The torque T_3 is characterized by a nonlinear transfer function. Figure 16 is the block diagram representation of the coulomb friction effect. Multiplying $\dot{\theta}_3(s)$ by $L/2\pi$ gives the Laplace transform of the table velocity, $\dot{X}(s)$. Then comes the nonlinear block representing the coulomb friction, its output is $F_3(s)$, the Laplace transform of the resultant of the friction forces induced in the slideways; physically the force F_3 causes a uniform axial loading in the lead screw and thus induces the torque T_3. The relation between F_3 and T_3 is the same as between the cutting effort, F_x, and the corresponding torque T_1, i.e.

$$T_3 = K_1 F_3 \tag{13}$$

The torque T_4 required to accelerate the screw in rotation is

$$T_4 = J\ddot{\theta}_3 \tag{14}$$

with J, the inertia of the screw and $\ddot{\theta}_3$, the acceleration of the angular displacement of the lead screw at position 3, defined as previously.

The Compression Strength F. It is the summation of

1. F_1, the force due to the cutting effort.

2. F_2, the force due to a viscuous friction in the screw and nut transmission.
3. F_3, the force due to a nonlinear coulomb friction in the slideways.
4. F_4, the force required to accelerate the table-workpiece assembly.

The force F_1 is the resultant of the uniform axial loading of the lead screw caused by the cutting effort; its magnitude equals the magnitude of the cutting effort F_x defined by equation (2),

$$F_1 = F_x = K\left[x\left(t - \frac{1}{zf}\right) - x(t)\right]$$

A rough estimate of the friction force, F_2, is obtained for the simplified type of lead screw already defined in Figure 14. The study of the equivalent problem of a mass sliding on a slope, as represented in Figure 15, shows that F_2 is the projection of the friction force, F_v, in the x-direction, i.e. on the axis of the lead screw. Thus it comes

$$F_2 = F_v \cos \varphi$$

or with substitution of equation (11)

$$F_2 = KA \frac{L}{2\pi} \dot{\theta}_3 \cot \varphi = K_2' \dot{\theta}_3 \qquad (15)$$

where K_2' is a constant.

The force F_3 has already been defined in the preceding paragraph; Figure 16 is a block diagram representation of the coulomb friction, i.e. of the cause of F_3.

The force F_4 required to accelerate the table-workpiece assembly is

$$F_4 = \frac{ML}{2\pi} \ddot{\theta}_3 \qquad (16)$$

with M, the mass of the table-workpiece assembly; L and θ_3 represent the same physical values as in previous paragraphs.

Interfacing of Cutter Rotation and Table Displacement

The Load Torque Applied to the D. C. Motor

As seen previously in this chapter, the load torque to which the cutter and spindle are submitted is defined by Equation 4 which is modified as follows:

$$T_L = K'\left[x\left(t - \frac{2\pi n}{z\dot{\theta}_m}\right) - x(t)\right]$$

with x the function describing the table displacement, $\dot{\theta}_m$ the speed of rotation of the D. C. motor shaft, n the reduction ratio between the D. C. motor rotation and the spindle rotation and z the number of teeth of the cutter. This notation is summarized in Figure 17. If J_e and B_e represent the inertia and damping coefficients of the single variable system equivalent to the motor and gear combination, there comes the incomplete block diagram representation shown in Figure 18; this model assumes the following series expansion (11),

$$x\left(t - \frac{c}{\dot{\theta}_m}\right) = x(t) - \frac{c}{\dot{\theta}_m}\dot{x}(t) + \frac{C^2}{2\dot{\theta}_m^2}\ddot{x}(t)$$

with $c = \frac{2\pi n}{z}$.

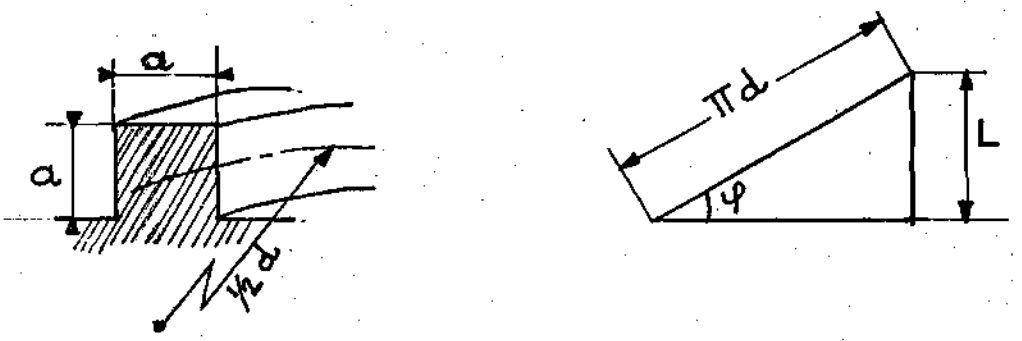

Figure 14. Definition of the Simplified Type of Thread.

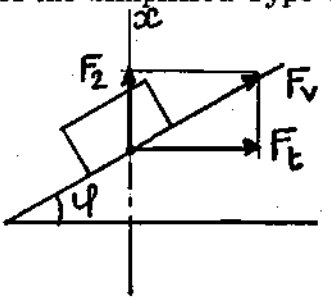

Figure 15. Viscuous Friction Force Applied to the Lead-Screw Equivalent Problem.

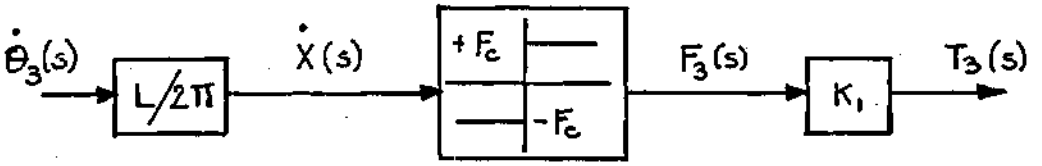

Figure 16. Nonlinearity due to the Coulomb Friction.

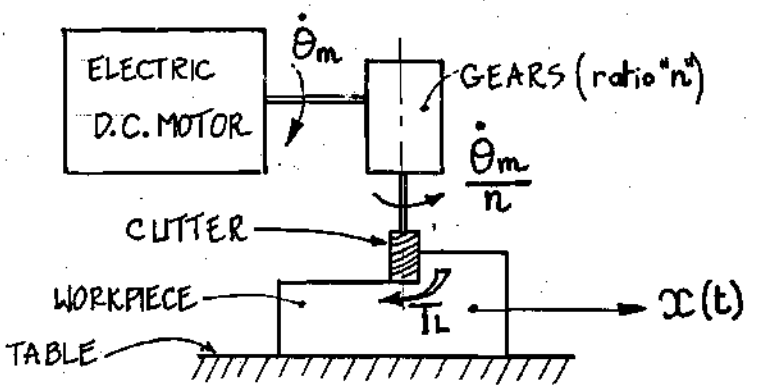

Figure 17. Load Torque Influence on the D. C. Motor.

The products of two time-domain functions

$$\dot{x}(t) \text{ by } \dot{\theta}_m^{-1}$$

$$\ddot{x}(t) \text{ by } \dot{\theta}_m^{-2}$$

could be Laplace transformed using the complex convolution integral definition, as shown in Appendix B. This method would be difficult to employ and it is recommended that the system be simulated on an analog computer; one could use the Quarter Square Multiplier, as described in Appendix C. Figure 19 gives the base for a computer setup.

A Simplified Model

The major difficulty to overcome in the modeling process appears in Equations (2) and (10) giving the expressions of F_1 and T_1

$$F_1 = F_x = K\left[x\left(t - \frac{1}{zf}\right) - x(t)\right]$$

$$T_1 = K_1 K\left[x\left(t - \frac{1}{zf}\right) - x(t)\right]$$

Here x is a function of time and of "f" which is itself a function of time. As in the preceding paragraph, the use of a series expansion would be the best approach for a detailed mathematical analysis. Figure 20 allows one to have a physical understanding of the problem: the table displacement and the cutter rotation (or its frequency f) are function of the cutting load which is itself a function of the table displacement and cutter rotation. Assuming a sufficiently powerful D. C. motor

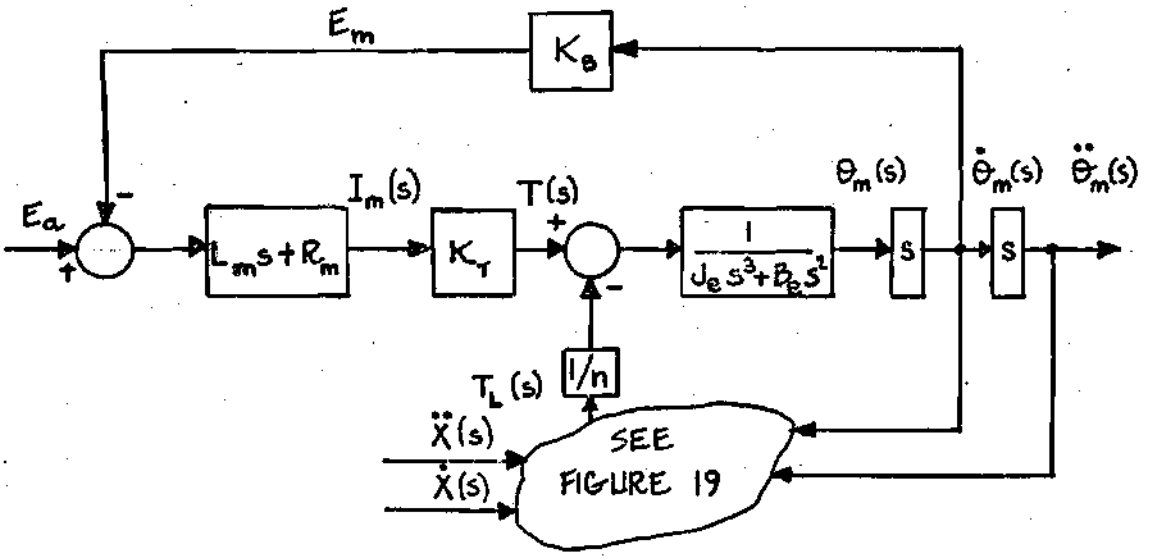

Figure 18. Block Diagram Representation of the D. C. Motor, Gears and Spindle System.

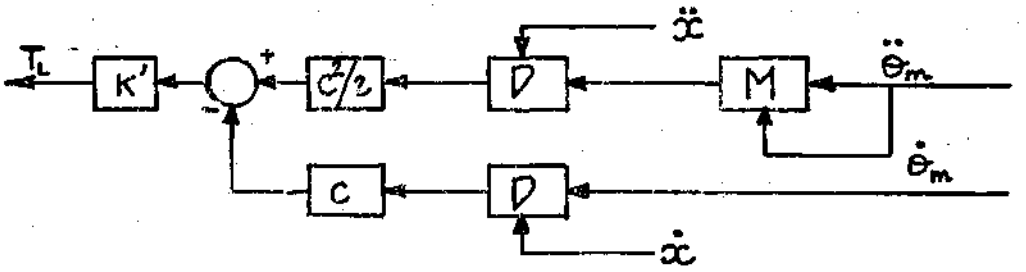

Figure 19. Computer Setup for the Simulation of the Missing Transfer Function in Figure 18.

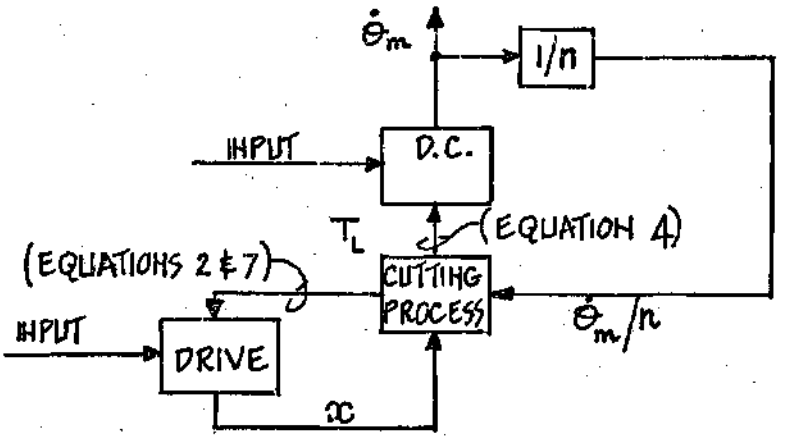

Figure 20. Feedback Loops of the Cutting Process.

to overcome the cutting load, with a small sensitivity to the load variations, is a reasonable simplification of the problem. If "f" is considered to remain constant, the following expressions can be written, applying the Laplace transform

$$F_1(s) = K\left[e^{-\frac{s}{zf}} - 1\right] \cdot X(s) \tag{17}$$

$$T_1(s) = K_1 K\left[e^{-\frac{s}{zf}} - 1\right] X(s) \tag{18}$$

Stiffness Coefficients and Lead Screw Deflections

Equation 6 introduced K_A and K_T, the axial and torsional stiffness of the lead screw, respectively. In Appendix A, K_A and K_T have been computed for a fixed length of the screw. A more sophisticated analysis shows that the length to be considered in the computation of K_A and K_T is the portion of the screw comprised between positions 1 and 2, as defined in Figure 7. This length is time varying and can be measured by the table displacement x(t), or x(t) plus a constant. As K_A and K_T are proportional to 1/x(t), the following expressions for the axial and torsional deflections of the screw can be written

$$\Delta_A \theta = k_A F \cdot x \tag{19}$$

$$\Delta_T \theta = k_T F \cdot x \tag{20}$$

with k_A and k_T, two constants. The product of the two time-domain functions x(t) and F(t) could be Laplace transformed using the complex convolution integral definition given in Appendix B. As this method would lead to a complex

mathematical analysis, a simulation on an analog computer and the use of the Quarter Square Multiplier of Appendix C are recommended.

If, during a specific machining operation, the table displacements remain very small compared to the length of the portion of lead screw between position 2 and position 3, it is time saving to start with an approximate analysis under the assumption that the stiffness coefficients of the screw remain constant. Thus Equations 19 and 20 would be simplified by replacing the time varying function x(t) by a constant value x_o.

Block Diagram Representation of the Lead Screw Transmission

Enough elements have been studied to draw the block diagram representation shown in Figure 21. The input is θ_2, while the output is x; two groups of feedback loops, the torques and the axial efforts, allow the evaluation of the angular deflection of the screw; this value subtracted from the input θ_2, gives the angular displacement of the screw at position 3, the only position where the angular displacement of the screw and the linear displacement of the table are related by a constant transfer function

$$X(s) = \frac{L}{2\pi} \theta_3(s)$$

or in the time domain

$$x(t) = \frac{L}{2\pi} \theta_3(t) \qquad (8)$$

This model has been established under the assumption leading to the approximate expressions given by Equations 17 and 18.

List of Symbols and Reference to Their Origin

F	Resultant of the forces inducing a uniform axial loading of the lead screw
F_1	Resultant of the uniform axial loading of the lead screw due to the cutting effort
F_2	Resultant of the uniform axial loading of the lead screw due to the viscuous friction between nut and screw
F_3	Resultant of the uniform axial loading of the lead screw due to the coulomb friction in the slideways
F_4	Resultant of the uniform axial loading of the lead screw due to the acceleration of the table
f	Frequency of the cutter rotary motion
J	Inertia of the lead screw
K	Constant Coefficient (defined in Equation 2)
K'	Constant Coefficient (defined in Equation 4)
K_1	Constant Coefficient (defined in Equations 13, 10)
K_2	Constant Coefficient (defined in Equation 12)
K_2'	Constant Coefficient (defined in Equation 15)
K_A	Axial stiffness coefficient of the lead screw
K_T	Torsional stiffness coefficient of the lead screw
k_A	Constant Coefficient (defined in Equation 19)
k_T	Constant Coefficient (defined in Equation 20)
L	Lead of the thread in nut and screw
M	Mass of the table-workpiece assembly
s	Laplace operator
T	Total torque applied to the lead screw

T_1 Torque applied to lead screw due to the cutting effort

T_2 Torque applied to the lead screw due to the viscuous friction between nut and screw

T_3 Torque applied to the lead screw due to the coulomb friction in the slideways

T_4 Torque applied to the lead screw due to the acceleration of the screw

t Time

$x, \dot{x}$ Table displacement and table velocity, respectively

$\dot{X}(s)$ Laplace transform of table velocity

z Number of teeth composing the cutter

$\Delta_T \theta$ Deflection of lead screw due to torsional stiffness

$\Delta_A \theta$ Deflection of lead screw due to axial stiffness

θ_1 Angular displacement of the output shaft of the rotary hydraulic actuator

θ_2 Angular displacement of the lead screw at position 2 (defined in Figure 7)

$\theta_3, \dot{\theta}_3, \ddot{\theta}_3$ Angular displacement, velocity and acceleration of the lead screw, respectively, at position 3 (defined in Figure 7).

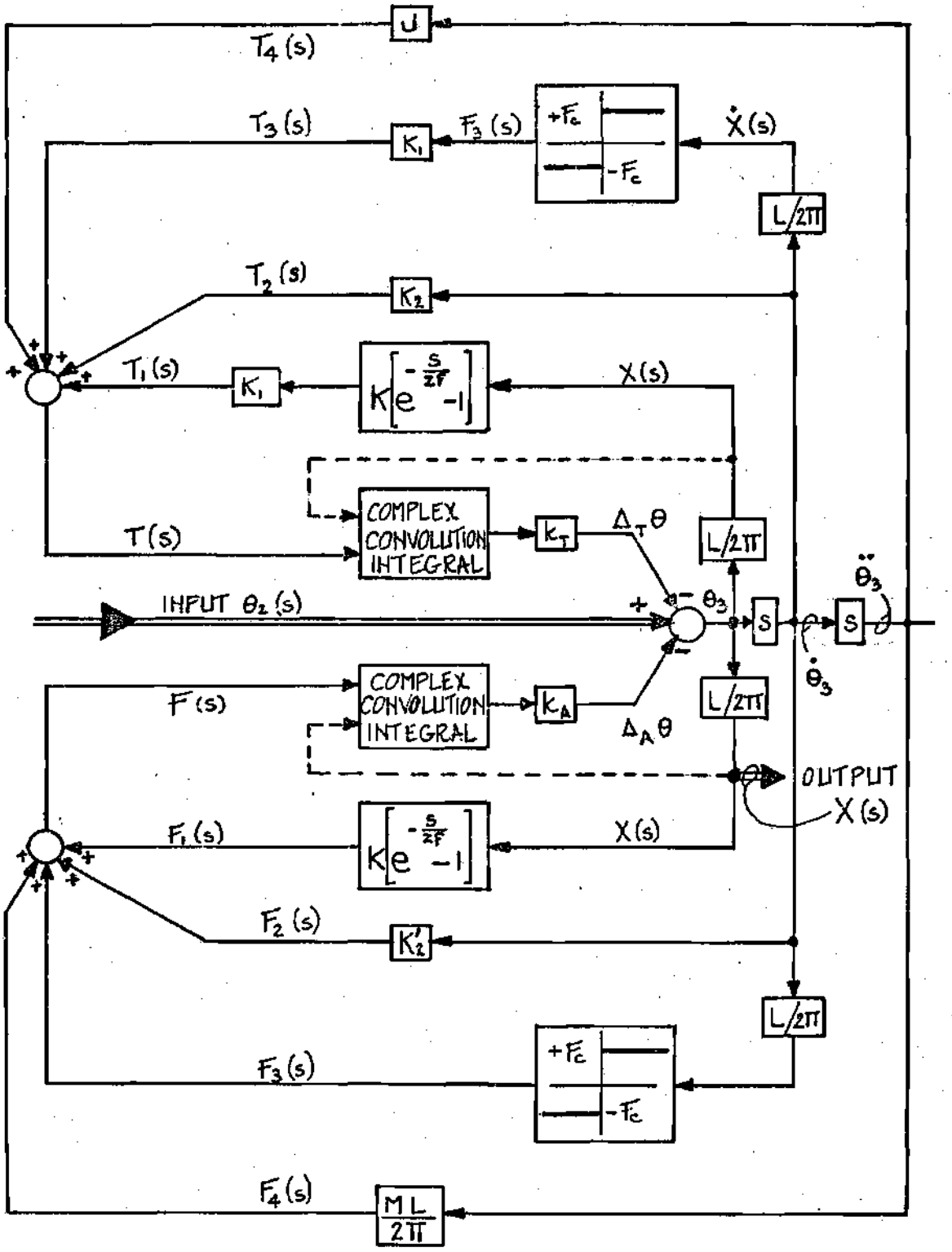

Figure 21. Block Diagram Representation of the Lead Screw Transmission.

CHAPTER III

MODELING OF THE ELECTROHYDRAULIC COMPONENTS

Why an Electrohydraulic Servodrive

For the servomotors the transient response is more important than the steady-state performance. Gille, Pelegrin, Decaulne (12) show that the design of a servomotor is based on its capacity to absorb and generate mechanical energy; therefore servomotors are always designed so that the inertias of their moving parts are minimized or, more precisely, that the ratio of inertia over mechanical torque is as low as possible. The ratio in size between a high pressure hydraulic pump and the electric motor required to run it can reach 1/10 (13). This has a significant bearing on automatic control for, as mentioned above, the inertias of the moving parts have an important influence on the response of the servodrive and therefore on the frequency range over which it can be used. By virtue of their low inertia, high-power hydraulic motors have a small time constant and thus a better response than their equivalent electric motors. Most of the main drawbacks of oil characteristics have been eliminated with today's products; the old-time foam trouble, the high temperature instability of the viscosity, the auto-inflammability danger and even the leakage problems have been reduced to a minimum. Another advantage of the hydraulic motor is that it may be repeatedly stalled by overloading without any damage.

When it is required to combine rapid response and high power, the hydraulic

system is best, but when the energy level remains low, electrical systems have an extremely high speed of response. Besides this, it should be noted that the classical hydraulic error-measurement devices are large and unable to perform the accuracy obtained with electronic devices, such as those using photoelectricity, LASER, inductance, etc. The above mentioned classical hydraulic error-measurement devices do not include the systems designed with fluidic components which can often compete with the solid-state electronic components. By selecting an electrohydraulic feedback control system, in which the electrical components handle the low energy signals (compensation networks, detectors ...) and the hydraulic components guarantee a high-power-to-weight ratio, one can usually obtain a high performance system combining the advantage of the two types of equipment. Figure 22 summarizes the various categories of hydraulic servo-drives. Type b-3 is a schematic drawing of the investigated system.

A Two-Stage Electrohydraulic Servovalve

This is the most commonly used type of electrohydraulic servovalve, it avoids the major drawbacks of the single stage type which are its limited flow capacity, due to the limited magnitude of the force available to stroke the spool, and its high sensitivity to the load dynamics. From the current literature (5, 14), a simplified two-stage hydraulic servovalve has been defined; as shown in Figure 23, the spool ends are under the pressure of stiff springs which act to center the spool against the pressure differential caused by the first stage; this first stage is of the flapper-nozzle type. The following notation will be used:

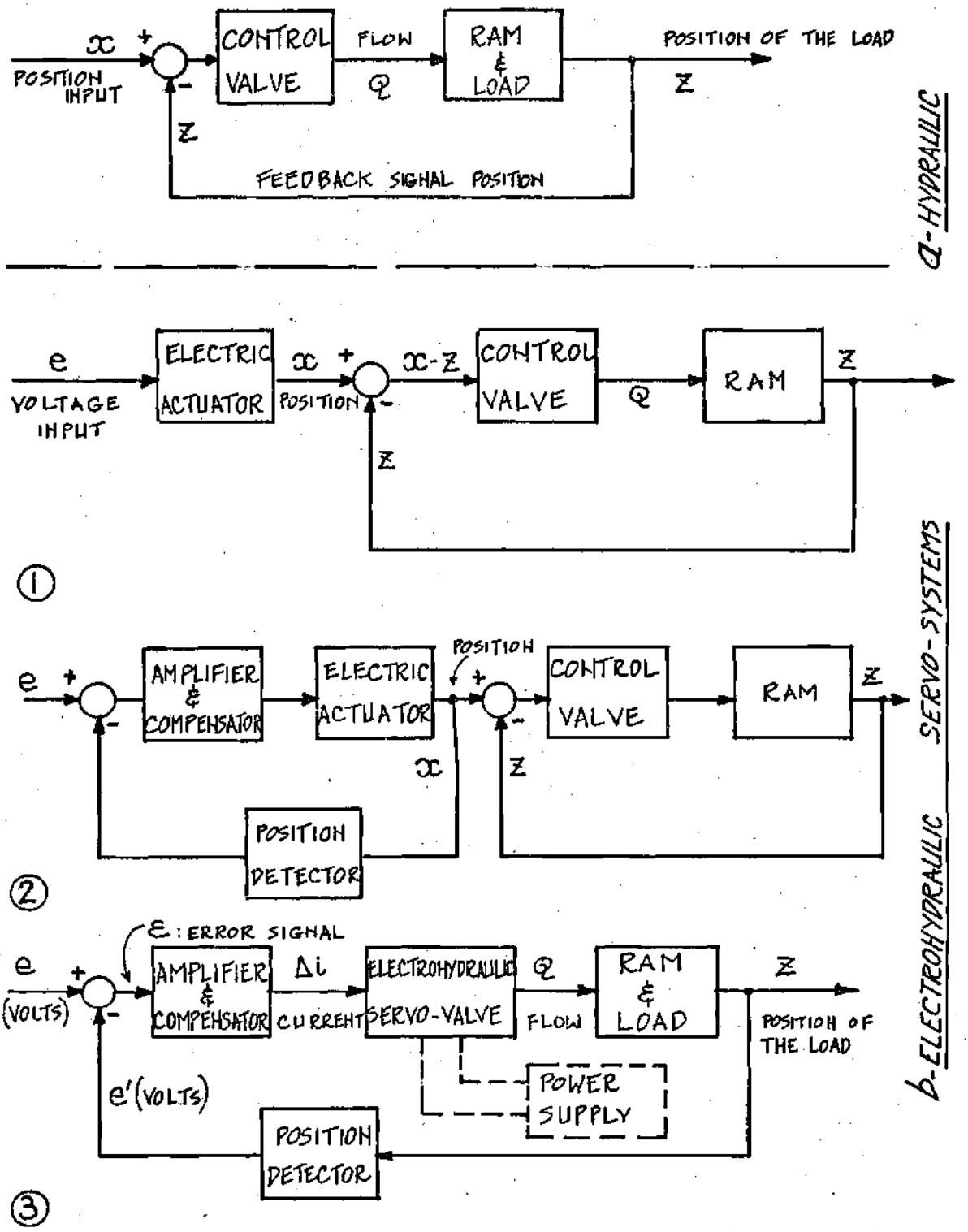

Figure 22. Several Types of Hydraulic Servodrives.

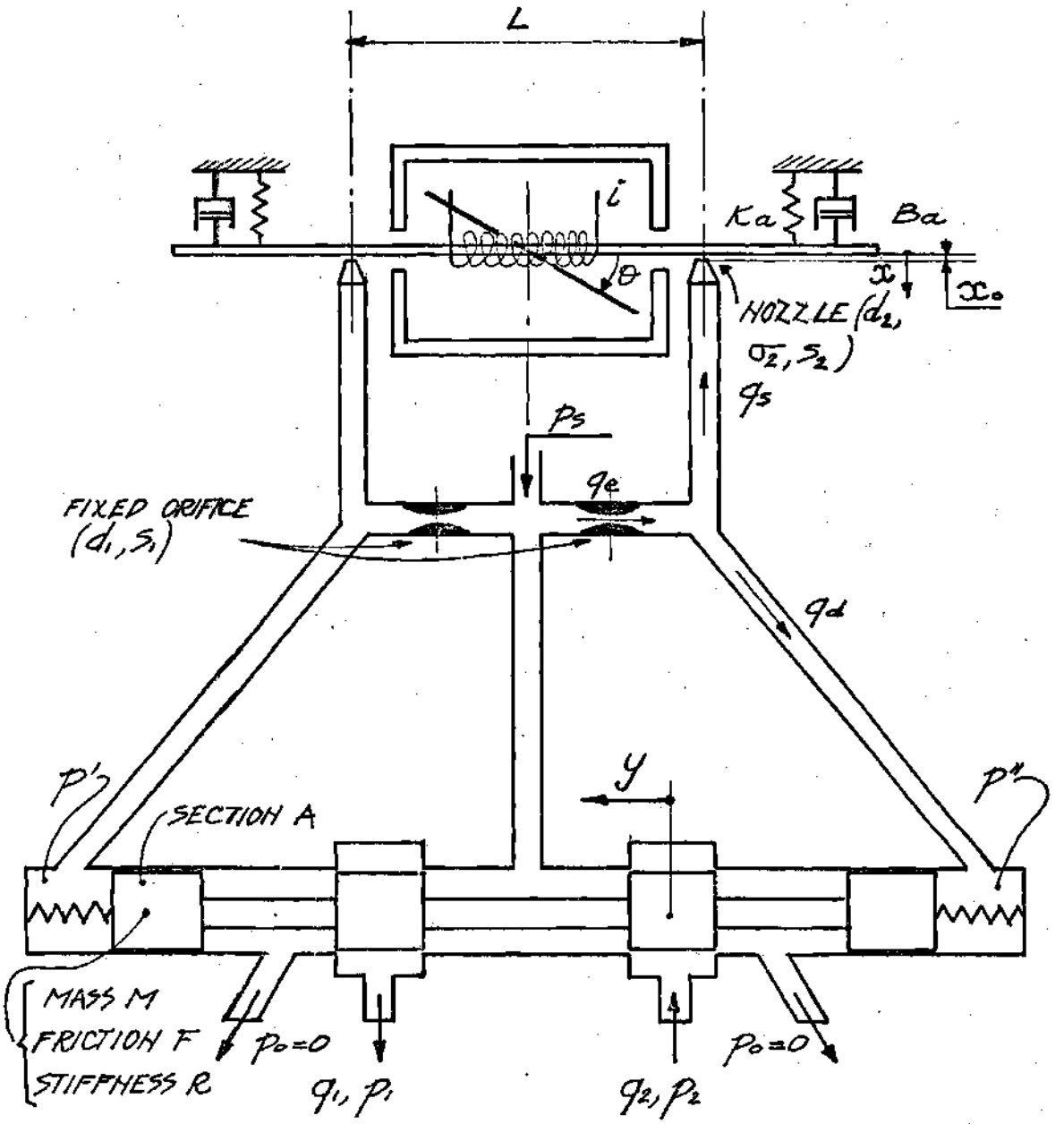

Figure 23. A Two-Stage Electrohydraulic Servovalve.

For the fluid:

β Bulk modulus

p_s Supply pressure

For the electrical stage (the flapper plate is the armature of the torque motor):

T_d Torque developed on the armature

i Current input

K_t Torque constant

K_m Magnetic spring constant

J_a Inertia of armature

K_a Rotational stiffness coefficient of armature

B_a Rotational viscuous friction coefficient of armature

For the first hydraulic stage:

θ Angle of rotation of the flapper-plate

L Distance between nozzles

x Deflection of flapper in direction of jet, $x = \frac{1}{2}\theta L$

x_o Distance between nozzle and flapper-plate at equilibrium position

d_2 Diameter of nozzle

σ_2 Cross-sectional area of nozzle

s_2 Area of fluid jet at nozzle

d_1, s_1 Diameter and section of fixed orifices

Pressure between fixed orifice and nozzle: if $i = 0$ $\frac{p_s}{4} = p_4$

$i \neq 0$ $\begin{cases} p'' = p_4 - p \\ p' = p_4 + p \end{cases}$

V Volume of fluid at pressure p' or p''

q_e, q_s, q_0 Flow thru hydraulic potentiometer at fixed orifice, nozzle and equilibrium position, respectively

For the second hydraulic stage:

A Diameter of spool

$\frac{R}{2}$ Stiffness of each spool end spring

F Viscuous friction coefficient of spool

M Mass of spool

y Displacement of spool from equilibrium position

The equations describing this system are the torque equation for the flapper plate, the force equation for the spool and the equation of the flow through the hydraulic potentiometer:

$$T_d = K_t i + K_m \theta - p L \sigma_2 \qquad (21)$$
$$= K_a \theta + B_a \dot{\theta} + J_a \ddot{\theta}$$

$$2Ap = Ry + F\dot{y} + M\ddot{y} \qquad (22)$$

$$q_e - q_s = A\dot{y} + \frac{V}{\beta}\dot{p} \qquad (23)$$

It can also be written,

$$q_e = k s_1 \sqrt{p_s - p''}$$

and

$$q_s = k S_2 \sqrt{p''}$$

which give after differentiation

$$\frac{dq_e}{q_o} = \frac{1}{2} \frac{d(p_s - p'')}{(p_s - p')_o} = - \frac{1}{2} \frac{p}{p_s - p_4}$$

and

$$\frac{dq_s}{q_o} = \frac{dS_2}{S_{20}} + \frac{1}{2} \frac{dp''}{p''_o} = - \frac{x}{x_o} + \frac{1}{2} \frac{p}{p_4}$$

thus it can be stated that

$$\frac{q_o p_s p}{2p_4(p_s - p_4)} + \frac{V}{\beta} \dot{p} - \frac{q_o}{x_o} x + A\dot{y} = 0$$

Replacing x by $\theta L/2$

$$\frac{q_o p_s}{2p_4(p_s - p_4)} \quad \text{by } \alpha$$

and $$\frac{Lq_o}{2x_o} \quad \text{by } \delta$$

gives $$\alpha p + \frac{V}{\beta} \dot{p} - \delta \theta + A\dot{y} = 0$$

Rewriting Equations 22, 23 and 24, using the Laplace Transform operator s, leads to

$$\theta = \frac{K_t I - L\sigma_2 P}{K_a - K_m + B_a s + J_a s^2} \tag{24}$$

$$P = \frac{\delta\theta - AsY}{\alpha + \frac{V}{\beta}s} \tag{25}$$

$$Y = \frac{2AP}{R + Fs + Ms^2} \tag{26}$$

where $\theta(s)$, $P(s)$, $Y(s)$ and $I(s)$ are the Laplace Transforms of $\theta(t)$, $p(t)$, $y(t)$ and $i(t)$, respectively. These three equations permit the block diagram representation shown in Figure 24, or its simplification shown in Figure 25. In this analysis the influence of the flow induced forces, also named Bernouilli forces, has been neglected. These forces are of two types:

1. The steady-state flow force due to the jet force through an orifice.
2. The transient flow force due to the acceleration of the fluid in the annular valve chamber.

This second type of force is of little significance to the valve dynamics (5). The first type of force has an axial component that tends to close the orifice of the valve chamber, as shown in Figure 26. This is similar to the action of a centering spring on the valve spool. This steady-state flow force F_j is directly proportional to the orifice area gradient w, the spool displacement y and the pressure drop through the orifice Δp; its direction is determined by the jet angle θ.

$$F_j = kwy\,\Delta p$$

The product (w·y) represents the orifice area. To stroke the spool, it is therefore

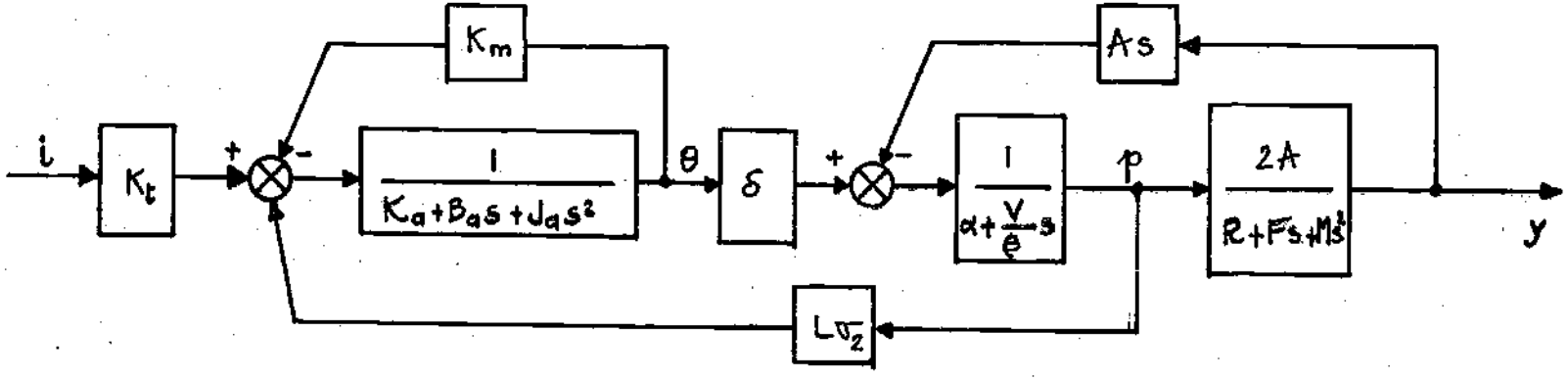

Figure 24. Block Diagram Representation of a Two-Stage Electrohydraulic Servovalve.

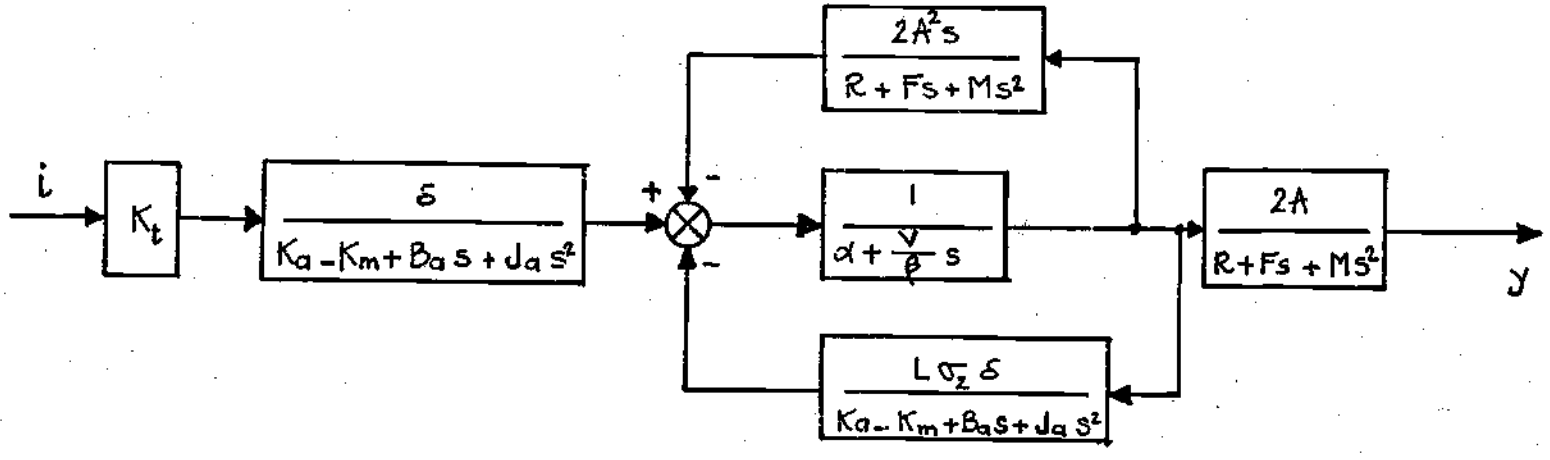

Figure 25. Simplified Block Diagram Representation.

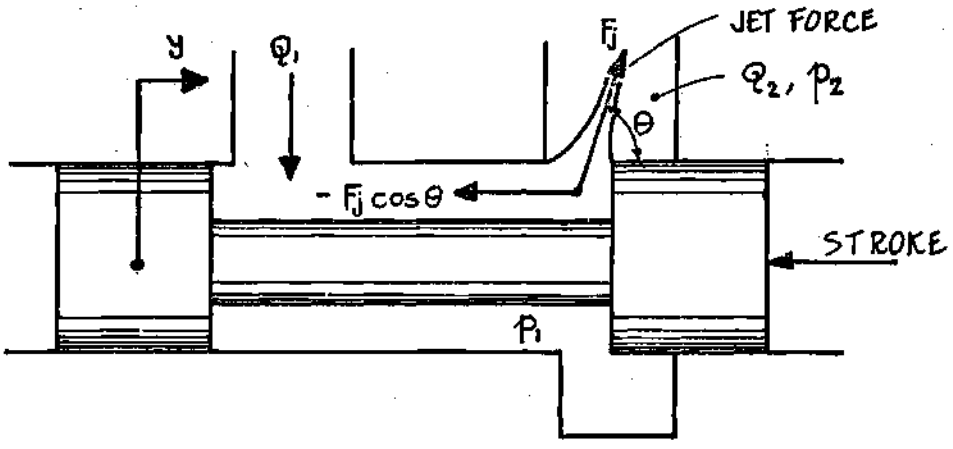

Figure 26. Steady-State Flow Forces Acting Upon a Spool Valve.

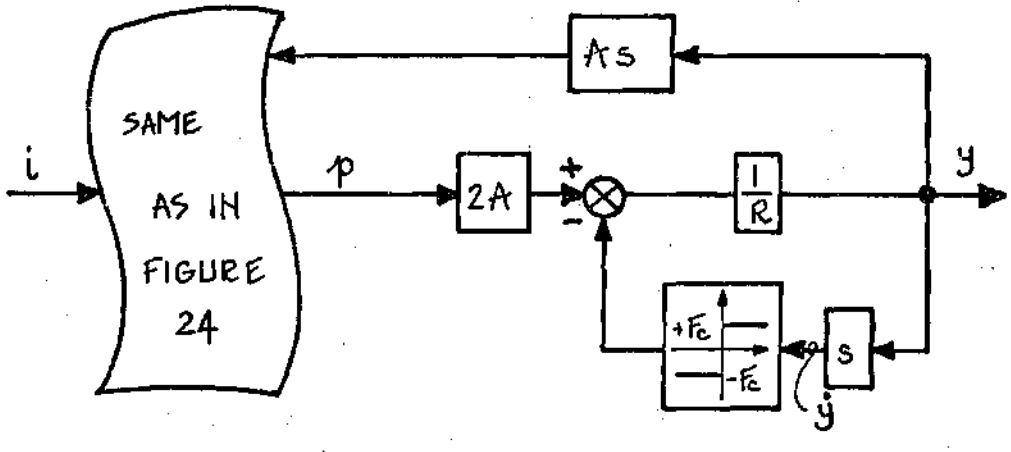

Figure 27. Coulomb Friction between Spool and Valve Chamber Walls.

necessary to apply an additional effort greater than $F_j \cos\theta$, the axial component of the jet force F_j. This consideration is fundamental for a single-stage valve but is of little significance for a two-stage device.

A servodrive must not be unstable; this is why it might be of interest to investigate the effect of a coulomb friction F_c in the valve chamber. In this case, an approximate preliminary analysis will neglect the viscuous friction in the chamber and the mass of the spool. Thus, a new equation can be written for the force combination acting upon the spool,

$$2Ap = Ry + F_c \qquad (27)$$

This equation allows the new block diagram representation shown in Figure 27.

The Amplifier and the Torque Motor

As seen in the preceding paragraph, the torque motor of the electrohydraulic servovalve is driven by a signal current i generated through a D.C. amplifier. Figure 28 shows how a signal voltage input e_g establishes the current i. R_1 is the input resistance of the amplifier, E_o its open circuit voltage and R_o its output resistance; i drives the parallel-mounted coils of the torque motor armature; each of these coils admits a current i/2; their resistance and self inductance are R_c and L_c, respectively; their mutual inductance is M. The angular displacement θ of the flapper plate creates a magnetic flux, thus there occurs a back e.m.f. proportional to $\dot{\theta}$; K_b is the back e.m.f. constant for each coil. It can be written that

$$E_o - iR_o = R_c\left(\frac{i}{2}\right) + K_b\frac{d\theta}{dt} + (L_c + M)\qquad \frac{d\left(\frac{i}{2}\right)}{dt}$$

If K is the gain of the amplifier

$$E_o = Ke_g$$

a substitution of E_o and the use of the Laplace Transform operator would give

$$e_g = \frac{1}{K}\left[\left(R_o + \frac{R_c}{2}\right)i + \left(\frac{L_c + M}{2}\right) si \right. \tag{28}$$

$$\left. + K_b s\theta\right]$$

A block diagram representation is given in Figure 29, with

$$R = R_o + \frac{R_c}{2}$$

$$L = \frac{L_c + M}{2}$$

As previously mentioned the feedback loop containing $K_b s$ is caused by the magnetic flux induced by the angular displacement θ. In Figure 24 there is another feedback loop, defined by the coefficient K_m, which is also caused by the magnetic flux induced by the angular displacement θ. Therefore, it is logical to use only one of those two feedback loops when analyzing the overall system composed of the amplifier, the torque motor, the flapper plate and the spool valve.

The Valve Controlled Hydraulic Rotary Motor

The system is illustrated by Figure 30. Assuming that the servovalve orifices are matched and symmetrical, the pressures in the lines will rise above

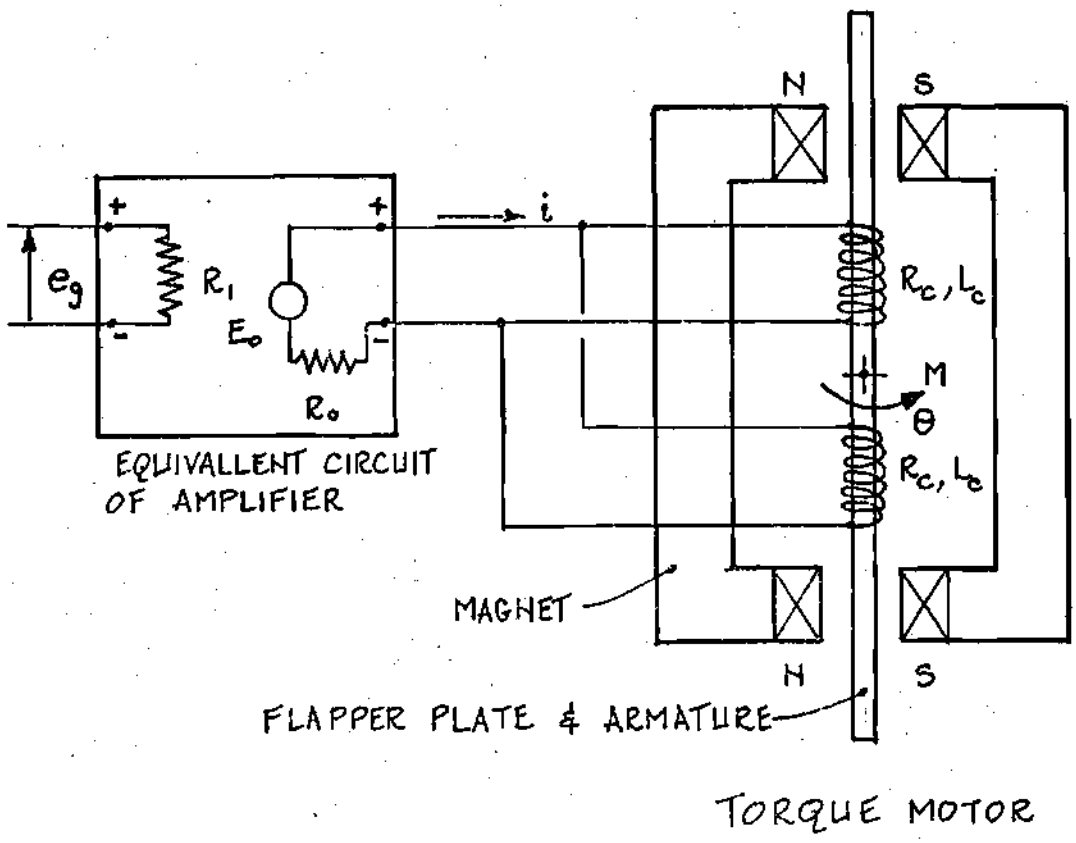

Figure 28. The D.C. Amplifier and the Torque Motor.

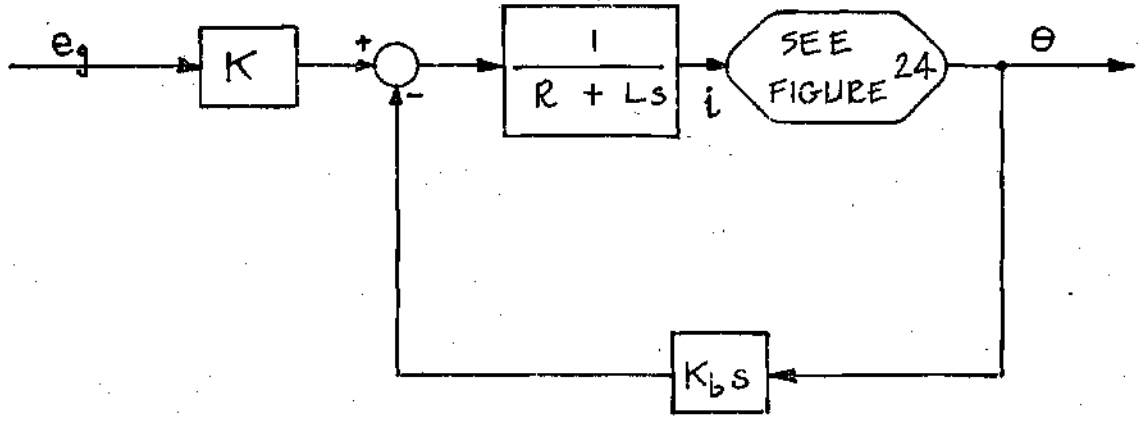

Figure 29. Block Diagram Representation of the Amplifier-Torque Motor System.

and below $p_s/2$ by equal amounts so that the pressure drops through the two orifices are identical and hence the valve coefficients for both flows are the same. The linearized servovalve flow equation is

$$q_L = K_q y - K_c p_L \tag{29}$$

with

$$q_L = \frac{q_1+q_2}{2} = \text{load flow}$$

$$p_L = p_1 - p_2 = \text{load pressure difference}$$

q_1 and q_2 are the forward and return flows, p_1 and p_2 the forward and return pressures, y the valve displacements from neutral, K_q the valve flow gain and K_c the valve flow-pressure coefficient.

After the valve equation, there comes the motor analysis; the description of a classical hydraulic rotary motor is available in current literature (5). Applying the continuity equation to each motor chamber allows Merritt (14) to obtain the Laplace transform of the load flow,

$$Q_L = D_m s\theta_1 + C_{tm} P_L + \frac{V_t}{4\beta_e} s P_L \tag{30}$$

where Q_L, P_L and θ_1 are the Laplace transforms of the load flow q_L, the load pressure difference p_L and the angular position θ_1 of the motor shaft; D_m is the volumetric displacement of the motor (in.^{3}/rad), C_{tm} the total leakage coefficient of the motor (in.^{3}/sec/psi), β_e the effective bulk modulus of the system (including oil, trapped air and mechanical compliance of the chambers) and V_t the total volume

of oil under pressure p_1 and p_2 (including the servovalve, motor chambers, connecting lines).

A third relation can be written to express the torque balance equation for the motor which, Laplace transformed, is

$$T_g = (P_1 - P_2)D_m = J_e s^2 \theta_1 + B_e s\theta_1 + T_L \qquad (31)$$

where T_g is the torque developed by the motor, J_e and B_e the equivalent inertia and viscuous damping coefficient of the motor and reduction gears referred to the motor shaft (as already described by Equation 15) and T_L the load torque on the motor. In the case of the machine tool presently studied, T_L is defined by

$$T_L = \frac{1}{n} T \qquad (32)$$

with n the reduction gear ratio and T the total torsion torque on the lead screw, already defined in Chapter III.

In Equation 31 the relation

$$T_g = D_m(P_1 - P_2)$$

defines an ideal generated torque; however there are other sources of torque losses which have been neglected; the most significant are:

1. The damping torque, proportional to the motor speed $\dot{\theta}_1$, required to shear the fluid in the small clearances between parts in relative motion. This effect is usually considered to define the value of the damping coefficient B_e.

2. The friction forces opposing motion of the piston; they cause an opposing friction torque proportional to the motor displacement and to the motor pressures. For steady state performance this torque loss is illustrated in Figure 31 and written as

$$T_f = \frac{\dot{\theta}_1}{|\dot{\theta}_1|} C_f D_m (p_1+p_2)$$

3. The negligible torque required to overcome the seal friction.

Equations 29, 30 and 31 allow the block diagram representation (14) shown in Figure 32.

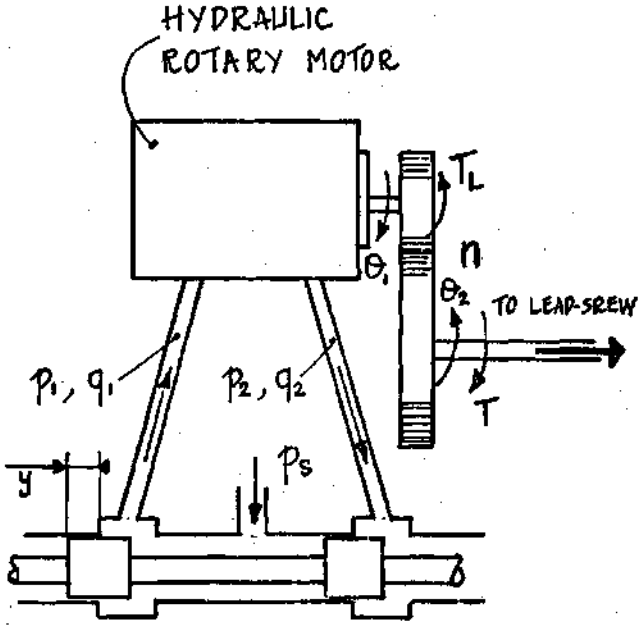

Figure 30. The Valve Controlled Hydraulic Rotary Motor.

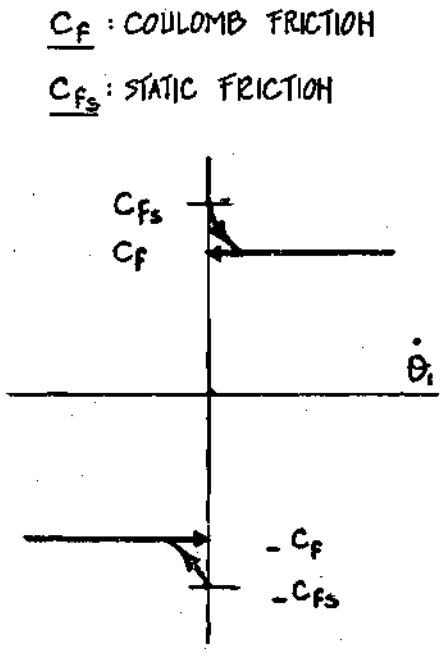

Figure 31. Coulomb Friction Nonlinear Torque.

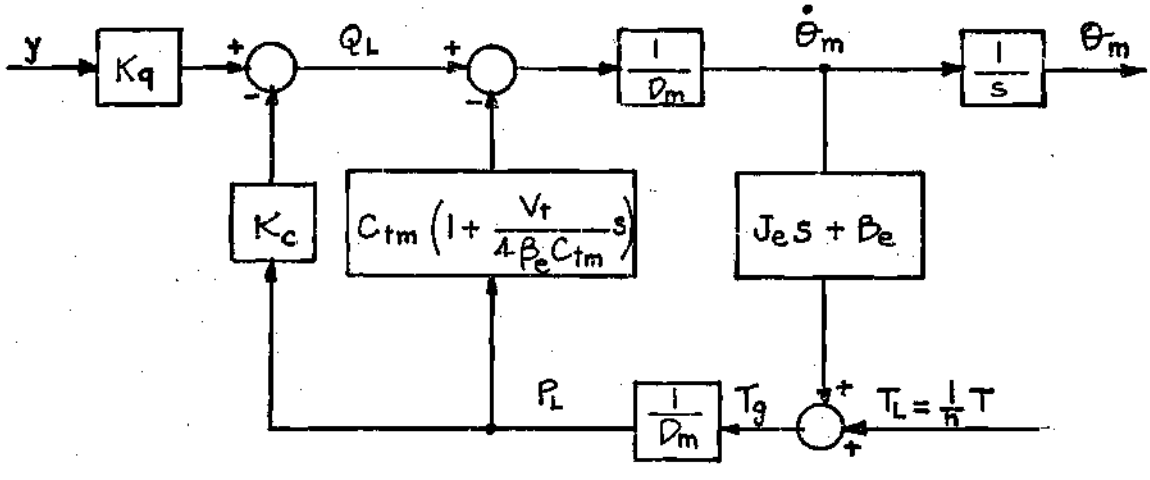

Figure 32. Block Diagram Representation of the Valve Controlled Rotary Motor.

CHAPTER IV

MODELING OF THE NUMERICAL CONTROL COMPONENTS

Description of a Typical Incremental Digital Feedback Control System

The block diagram (15) of such a position-control system is shown in Figure 33. Reference information R_A, consisting of the desired time response of the controlled variable θ, is processed through a reference quantizer, generating pulses which are then stored. Each pulse indicates that the magnitude of the controlled variable should change by one discrete element (quantum). Plus-pulses R^+_{pq} (or minus-pulses R^-_{pq}) are generated when the controlled variable is desired to increase (or decrease) by one quantum. These reference pulses are supplied to a bidirectional counter at a frequency indicative of the desired rate of change of the controlled variable. The number in the counter represents the instantaneous digital error existing between the actual value of the controlled variable and its desired value. The digital-analog converter produces a discontinuously varying analog error signal proportional to the number in the counter. This is the signal which is applied to the amplifier driving the electrohydraulic servovalve described in Chapter III. The rotary actuator, also described in Chapter III, modifies its position θ in response to the error signal. This actuator is mechanically coupled to the table of the machine tool through the lead-screw transmission, as described in Chapter II. In the particular case of the machine

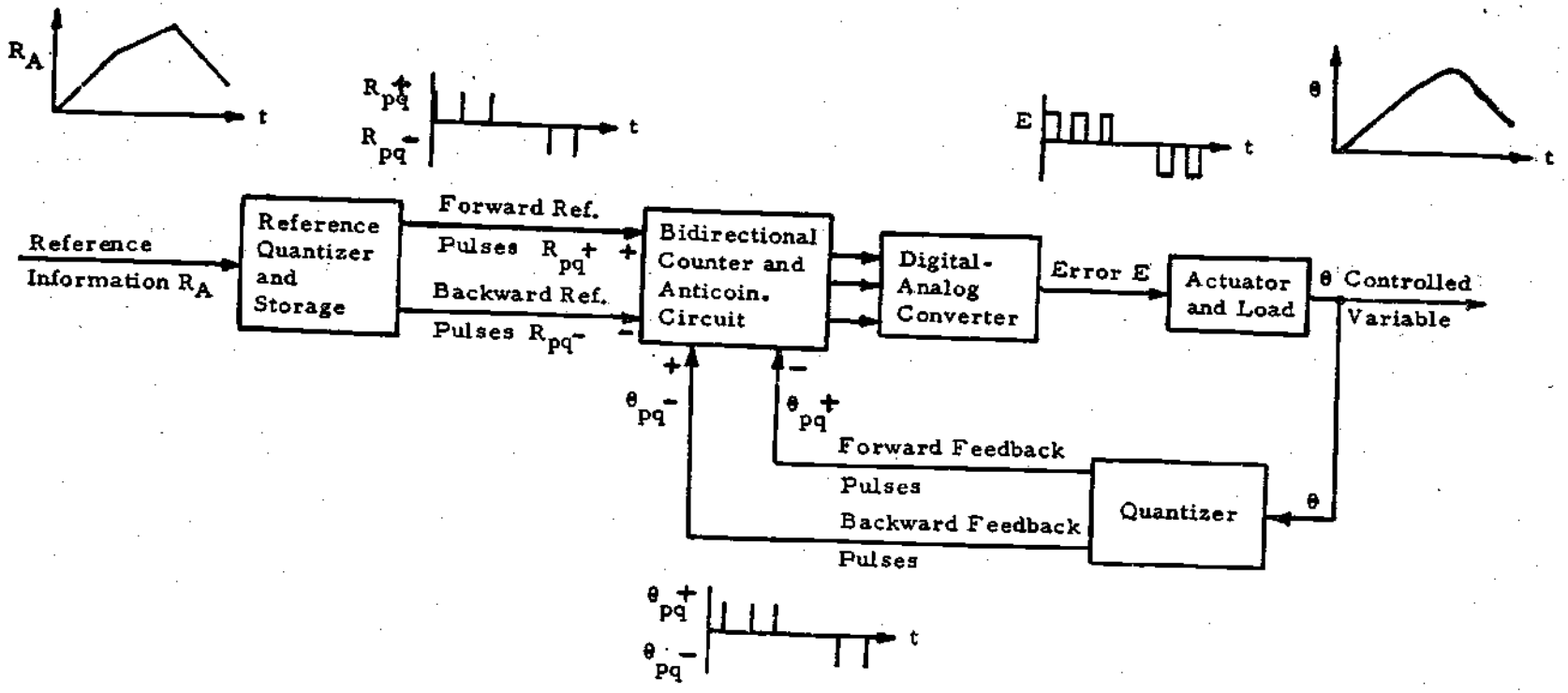

Figure 33. Block Diagram of a Typical Incremental Digital Control System.

tool there are two alternatives for the location of the feedback signal detector. If position is measured at the table, the control loop will include the lead-screw transmission and its nonlinearity, this might cause limit cycles. If feedback is taken from the hydraulic motor shaft, the nonlinearity will be outside the loop and this will cause a non-controllable error in the response. In both cases a quantizer, linear or angular, is coupled to the chosen element, table or motor shaft. This quantizer emits a plus-pulse θ^{+}_{pq} (or a minus-pulse θ^{-}_{pq}) each time that the magnitude of the controlled variable increases (or decreases) by one quanta value. Recall that a quanta is a discrete equal increment of the controlled variable, this is a function of the physical performance of the quantizer. For clarity, Figure 33 assumes that the feedback signal is taken from the motor shaft. An anticoincidence circuit avoids the loss of a pulse due to the possible simultaneous entrance of two distinct pulses.

A typical desired time response for the controlled variable is a "ramp" response. The input command for such a response consists of pulses equally spaced in time, the number of pulses represents the desired quanta change and their frequency represents the desired velocity in quanta per unit of time. With such a described system two major undesirable characteristics are observed, they are the result of the discontinuous pattern of the error signal: the actual time response of the controlled variable has a "staircase" pattern and its velocity assumes a limit-cycle mode; this is shown (15) in Figure 34.

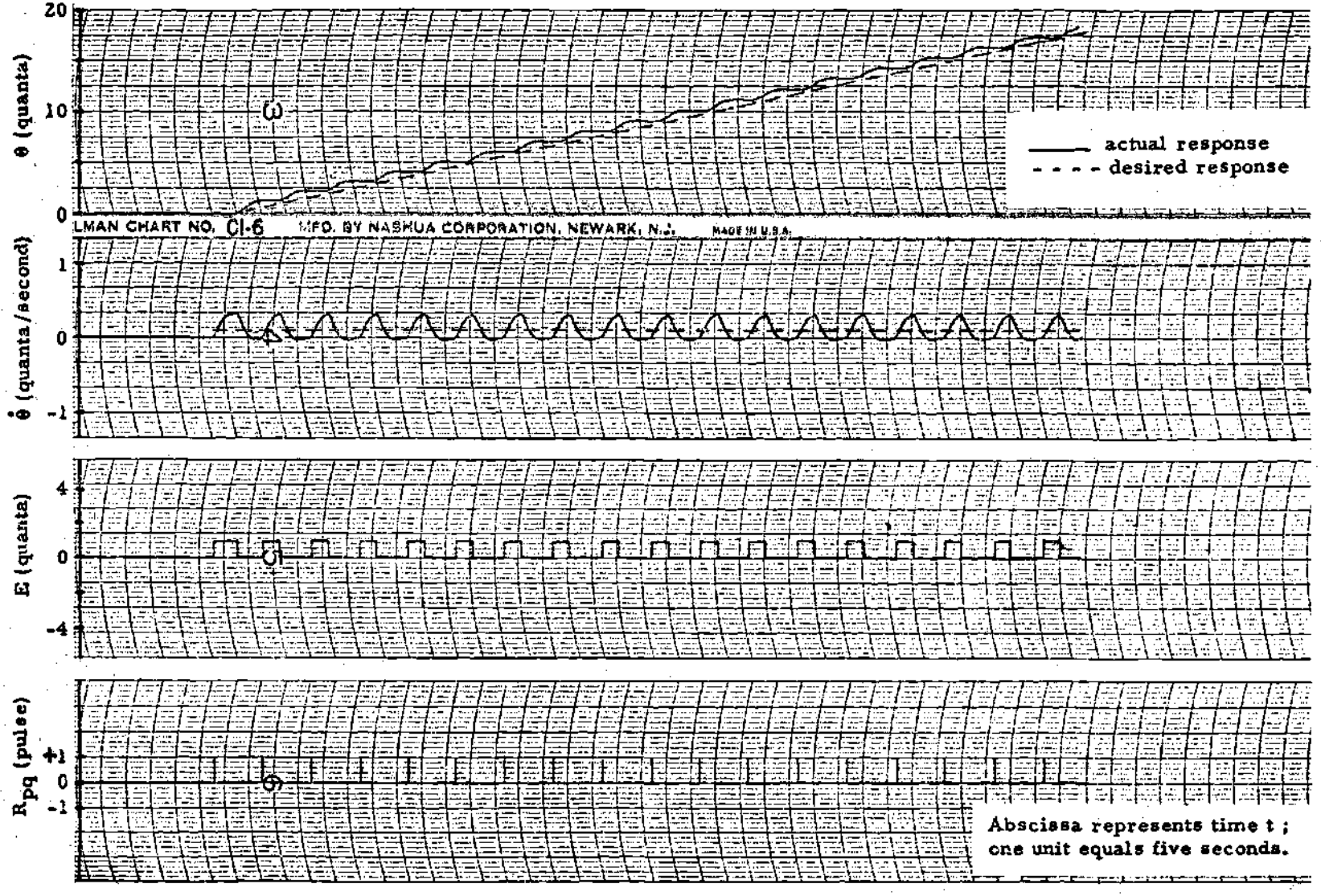

Figure 34. Ramp Response of the Controlled Variable θ of a Typical Digital Control System.

Description of a Compensated Digital Control System

The step-like response is very undesirable for the control of a machine tool because of the high-quality surface finish requirements. In order to minimize the undesirable step-like response, A. L. Holliman (15) developed a model of a compensated digital control system.

Compensation signals supplied with the pulse input signal and generated within the system provide a continuous reference-input signal R_c, a continuous feedback signal θ_c and, thus, a resulting continuous error signal E_c. Such a compensated system is shown in Figure 35, where R_d and θ_d are the digital components of R_c and θ_c, R_Δ and θ_Δ are the incremental components of R_c and θ_c. In Appendix D, Figure 48 shows how the compensation operates.

The advantages of such a compensated system is to retain the qualities of an uncompensated digital system, such as an easily transmitted digital input signal and a very accurate digital component in the feedback signal, while acquiring the "smoothness" of operation of a similar analog system.

A Simple Model

Figure 36 shows that the continuous reference input R_c is related to the reference information R_A by a transfer function of value 1.

Figure 37 shows that the continuous feedback signal θ_c is related to the actual controlled variable θ by a transfer function of value 1.

These graphs have been obtained by A. L. Holliman (15) on an analog computer while simulating his compensated digital control system. Therefore

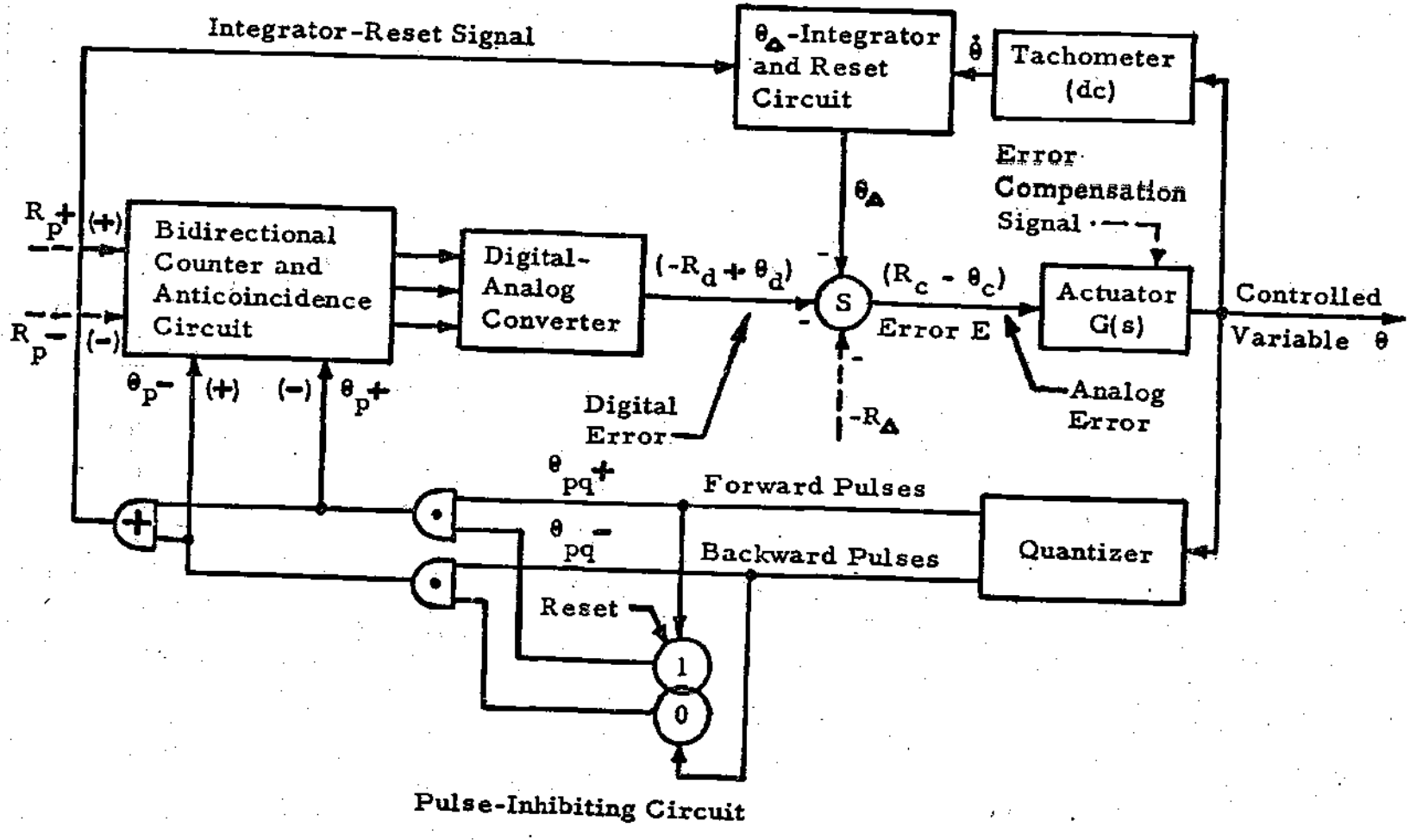

Figure 35. Actuator, controlled-variable, and feedback paths for the compensated digital control system.

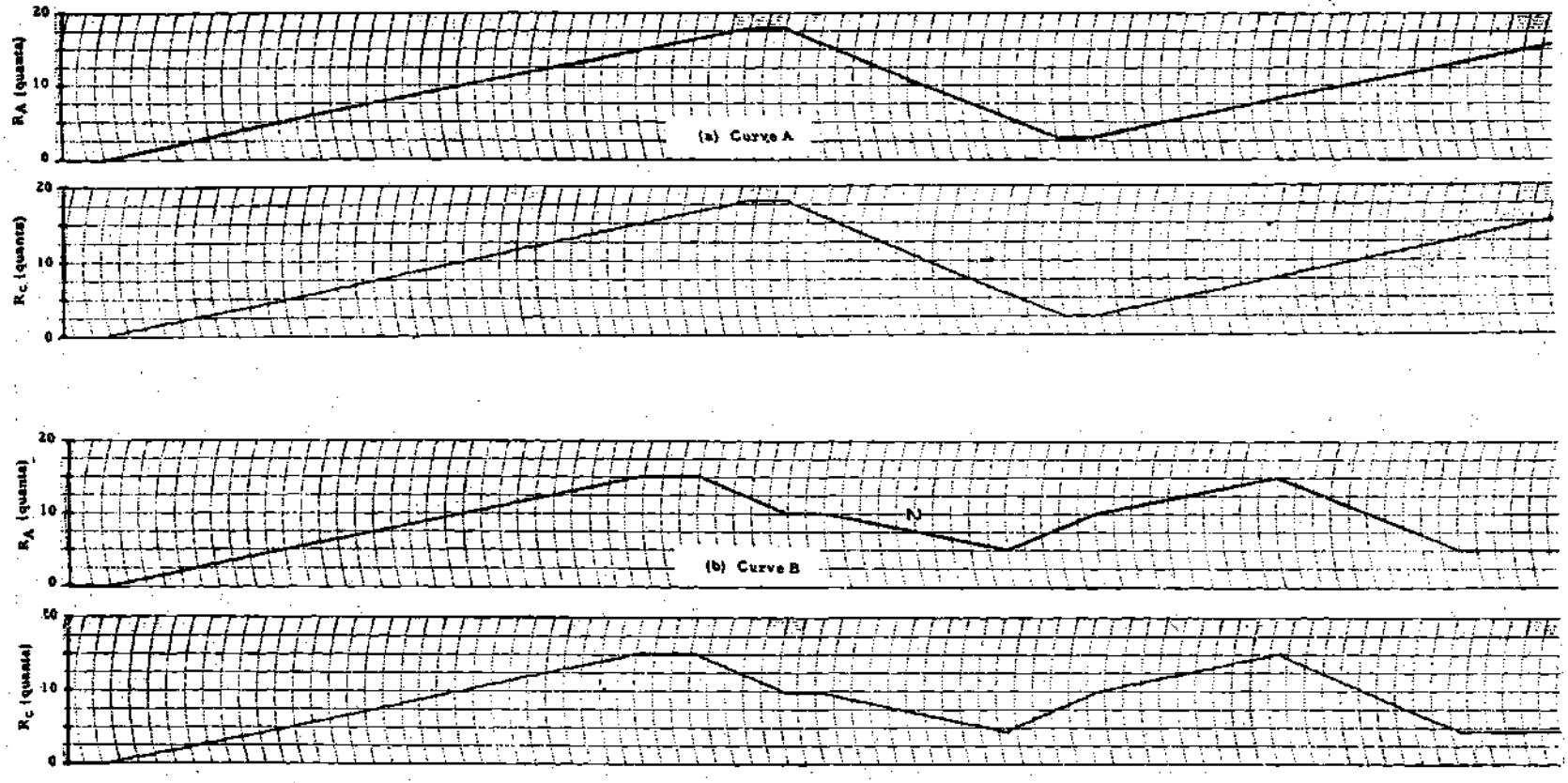

Figure 36. A Typical Reference Information R_A and the Corresponding Generated Continuous Reference Input R_c.

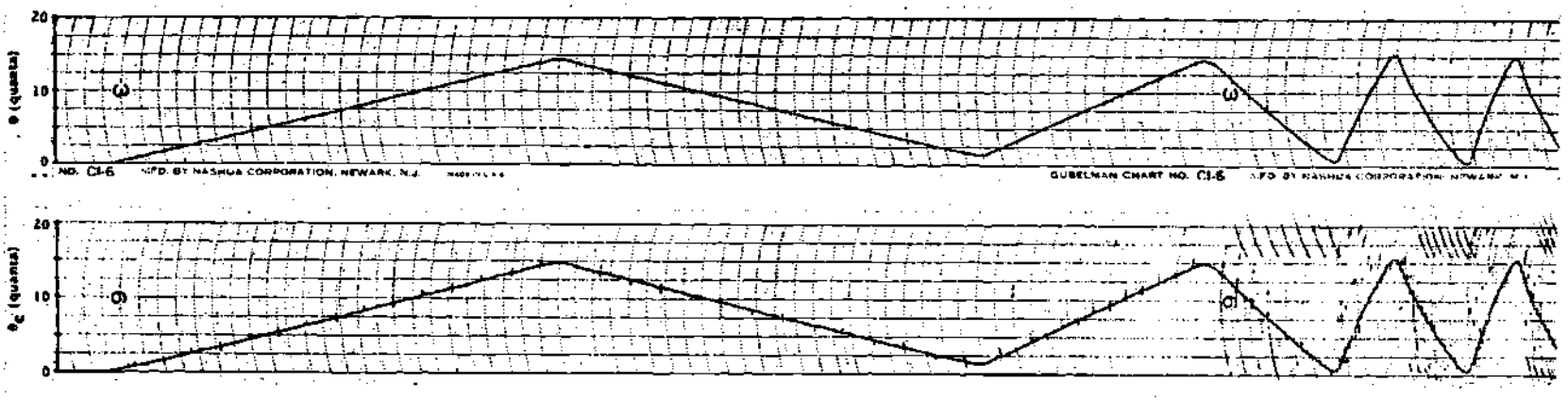

Figure 37. A Typical Controlled-Variable Time-Response θ and the Corresponding Generated Continuous Feedback θ_c.

$$E = R_c - \theta_c$$

can be replaced by

$$E = R_A - \theta$$

Another formulation of this result is that all the following elements

- Bidirectional counter
- Anticoincidence circuit
- Digital-analog converter
- Feedback quantizer
- Compensation circuits (tachometer, integrator, reset circuit, pulse-inhibiting circuit)

are assumed to be represented by the transfer function of constant value k, as shown in Figure 38.

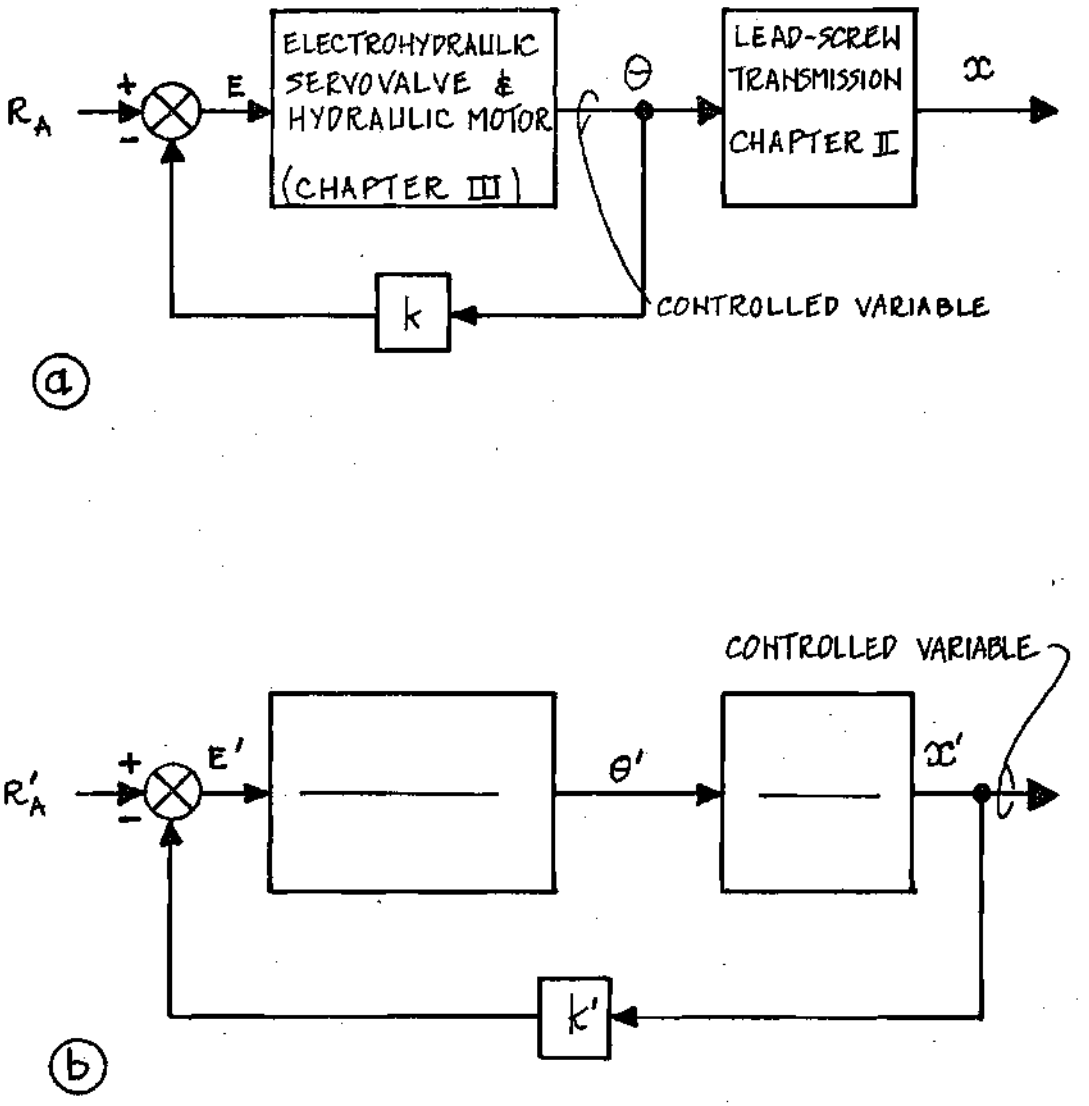

Figure 38. Block Diagram Representation with a) Feedback Taken from Motor Shaft, b) Feedback Taken from Table.

CHAPTER V

ANOTHER TYPE OF COMPENSATION: THE DIGITAL LEAD COMPENSATOR

The digital lead compensator, described here, manipulates the error signal of the incremental digital positioning system, described in the preceding chapters, while it is still in a digital form. As already mentioned, the use of a compensation device is required by the discontinuous nature of the feedback signal which might make the classical control system, shown in Figure 33, difficult to stabilize. In effect, the control variable is represented in the control system only when a feedback pulse is generated by the quantizer; the system runs open-loop the rest of the time.

Digital Approximation of an Analog Derivative Action

The derivative response of a classical analog lead compensator can be approximated by a digital control network whose response is the sum of two step functions, as shown in Figure 39. The compensator output, for a step input, is given by

$$E(t) = (a+1)u(t) - a\,u(t-T)$$

where u(t) is the unit step function at time t=0 and "a" is the amplitude of the pulse superimposed on the proportional uncompensated output, T is the pulse width. The Laplace transforms of the output and input lead to the transfer function

$$C(s) = a + 1 - a\, e^{-Ts}$$

or with $s = \sigma + j\omega$

$$C(s) = a + 1 - a\, e^{-T\sigma}(\cos T\omega - j \sin T\omega) \tag{33}$$

This transfer function C(s) has no finite poles; its zeros may be found by separating the real and imaginary parts of Equation 33 and setting them equal to zero. The zeros added by the compensator are given by

$$Z_k = \frac{1}{T} \ell n \frac{a}{a+1} + j \frac{2k\pi}{T} \tag{34}$$

$$k = 0, \pm 1, \pm 2 \text{ etc....}$$

Since "a" and T are greater than zero, the real part of those zeros Z_k is always negative, this shows that all the zeros lie in the left-half of the s-plane.

In the frequency domain, $C(j\omega)$ is obtained for σ approaching zero

$$C(j\omega) = a + 1 - a \cos T\omega + ja \sin T\omega \tag{35}$$

If the value of T is small enough, the following approximations can be written

$$\sin \omega T = \omega T$$

$$\cos \omega T = 1$$

Substituting these approximated values into Equation (35) gives

$$C(j\omega) = 1 + ja\, T\omega \tag{36}$$

The compensator consists of two one-shots which provide a pulse of width T with each positive or negative counter input pulse, as shown in Figure 40. If two pulses arrive at the input of a one-shot within the interval of time T, the second pulse will not register and the compensation effect will be lost. Thus, T must be chosen smaller than the time between command pulses when emitted at the maximum possible rate.

Improvement of the System Stability

As seen previously, the compensator adds an infinite number of zeros to the system. Neglecting the zeros which are far from the system poles limits the study to the influence of the only significant zero, the one at

$$s = \frac{1}{T} \ln \frac{a}{a+1} \tag{37}$$

As the pulse height "a" increases, the significant added zero approaches the origin and the loci branches bend to the left, away from the imaginary axis, thus increasing the maximum allowable gain to keep the system stable (16).

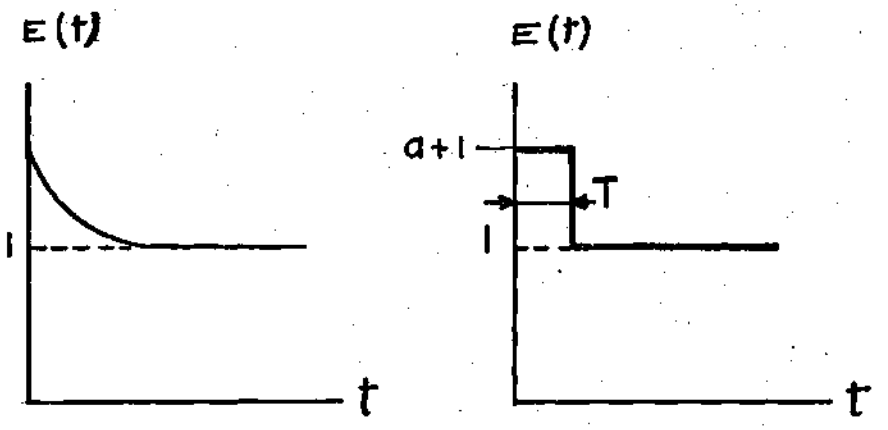

Figure 39. Digital Approximation of an Analog Derivative Action.

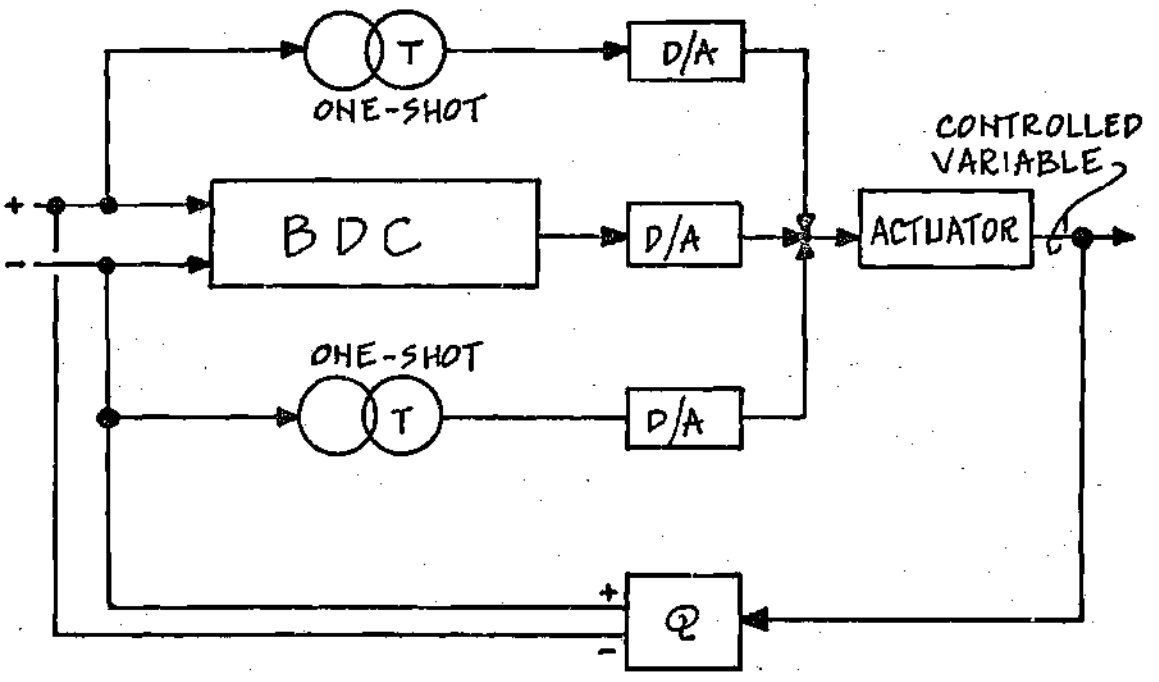

Figure 40. Digital Lead Compensator.

CHAPTER VI

INFLUENCE OF STRUCTURE DEFLECTIONS

This chapter formulates problems which could be investigated in further studies. In the preceding chapters, the bed structure of the machine tool was assumed to be of perfect rigidity while chatter perturbations were neglected.

Bed Deflections

In many cases bed deflections must be considered since the position detector is usually suspended between a part of the bed structure and the table. The analysis of a machine tool structure is too complex to be developed here; but the block diagram representation of Figure 41 shows what modification, in the aspect of the control loop, is expected.

Chatter as a Feedback Loop

Chatter is a violent vibration caused by the interaction between the metal cutting process and the machine tool structure; it can be explained by a feedback process (17) which is shown in Figure 42. The feedback path transfer function is shown as a delay because, as the structure deflects, the tool is removed from the workpiece leaving a lump on the cut surface and this lump must be removed by the next cutting tooth; in effect, the structural deflection is multiplied by a delay term and added to the desired feed per tooth. In the case of multiple cutting, the feedback process is difficult to analyze because there is a transfer function for each

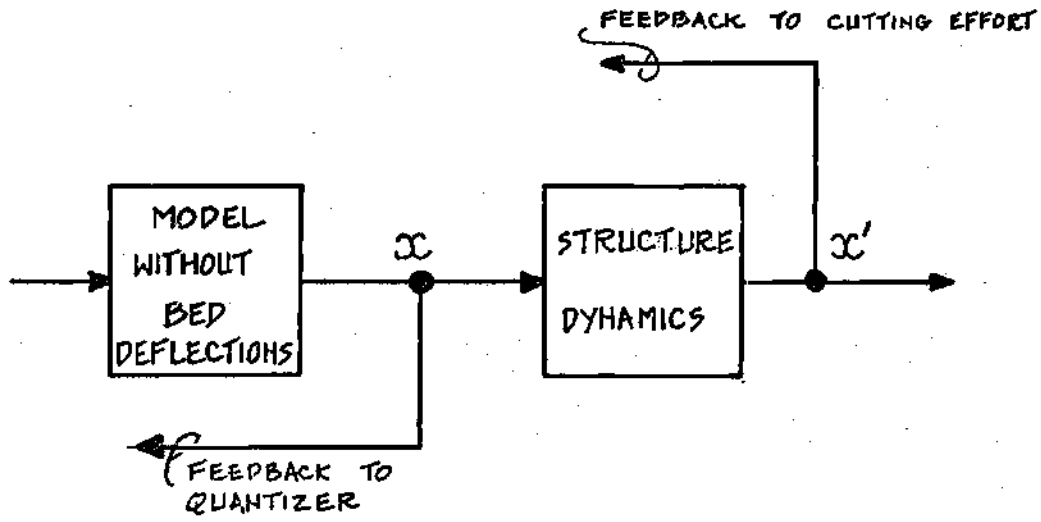

Figure 41. Influence of Bed Deflections.

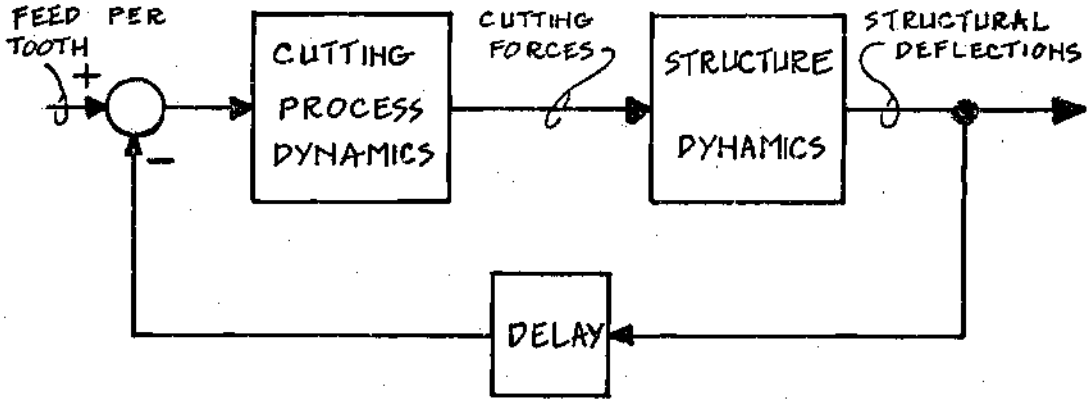

Figure 42. The Chatter Loop.

tooth in contact with the cut surface and these transfer functions have time varying coefficients due to the rotation of the cutter.

CHAPTER VII

CONCLUSIONS

Machine Tool Designer and Control Systems Engineer

Today's industry is demanding such high performance from machine tools that the mechanical designer and the control systems engineer are being forced into close cooperation. The study shows how both types of engineers can speak a common language: a modern numerically controlled machine tool is described as a multiple series of feedback loops.

In order to achieve completely the design of a high performance machine tool, the mechanical engineer and the control systems engineer will have to go further than the mathematical modeling steps developed here. They will investigate the problems suggested in Chapter VI: some large machine structures might have a significant influence on the dynamic characteristics of the servo-drive system, some of these structure resonances might even be affected by the type of foundation the machine rests on; the coupling of the chatter loop with the machine structure might also influence the overall performance of a numerically controlled machine tool.

Once the complete model is proposed, the cooperation will go on, and the mechanical engineer will provide the control systems engineer with actual values of the parameters (e.g., friction coefficients, valve dimensions, Young's modulus,

etc.) so that the form of the time response of the total system controlled variable can be defined. For the system under consideration, a simulation on an analog computer is recommended, particularly to avoid time-consuming mathematical studies required each time a convolution integral appears in the model.

Another type of approach could be conducted simultaneously, which would include the optimization of a few of the parameters, and thus the specification of the corresponding electromechanical or electrohydraulic characteristics, knowing the values of the others.

Nonlinear System Analysis

Generally speaking, a control system of the type under consideration may be designed to operate satisfactorily using linear theory and several requirements regarding system parameters may be deduced. However, when a high performance specification is to be satisfied, then the effect of various nonlinearities in the system must be understood before the optimum gain distribution can be approached. The describing function is a useful tool for dealing with single nonlinearities (18), but when several nonlinearities are acting simultaneously the use of an analog computer is desirable.

The following considerations allow some rough prediction--which needs to be verified by an analysis or a simulation--of the presence of limit cycle oscillations: many limit cycle oscillations within a servo system are due to simple mechanical static and sliding frictions. In a comprehensive study H. E. Merrit (19) defines three types of servo systems with friction,

a. - viscuous and friction forces dominant,

b. - inertia and friction forces dominant,

c. - spring and friction forces dominant.

He shows that the first two cases indicate no particular stability problem; it is only in the third case, where the friction forces are large compared with the forces needed to accelerate the load, that instability can be caused. This third case illustrates the "stick-slip" phenomenon; at low velocities a mass actuated by a compliant drive (e.g., the machine tool table actuated by a hydraulic rotary motor through a lead-screw transmission) may not move "smoothly" along the surface of contact (e.g., the guideways) but may exhibit a "jumpy" motion below a certain critical velocity.

The Next Generation of Machine Tools

To complicate the system already described, the machine tools of the next decade will have an Adaptive Control loop added to the present multiple loop system. In an adaptively controlled machine, sensors will be added to measure various parameters generated by the metal cutting process (e.g., temperature, torque, etc.), which will be then converted to some actual performance index of the overall machine tool system. This will be compared to a desired index and the adaptive controller will introduce correction signals to the numerical control director in order to modify the command input of the system.

APPENDICES

APPENDIX A

THE STIFFNESS COEFFICIENTS OF THE LEAD SCREW

The Axial Stiffness Coefficient

The Axial Stiffness of a Uniform Circular Bar

Assuming an elastic material, Hooke's law gives

$$\frac{F}{A} = E \frac{x_1 - x_2}{\ell}$$

where F is the compression force on the bar, A its circular cross section, E the Young's modulus of its material, (30×10^6 lb/in^2 for steel), x_1 and x_2 the displacements at its two ends and ℓ its initial length; this notation is illustrated in Figure 43. Assuming the bar to behave like a linear spring gives

$$F = k_A(x_1 - x_2)$$

with k_A, the axial stiffness coefficient of the bar defined as

$$k_A = \frac{EA}{\ell}$$

usually k_A is measured in lb/in.

The Axial Stiffness of a Schematized Lead-Screw

As a first approximation, the helical shape of the thread has been neglected;

a representation of the schematized screw is shown in Figure 44, thus the screw is considered as a series of circular elements assembled end to end. The axial stiffness coefficient of the screw, K_A, is such that its inverse, $(K_A)^{-1}$, is defined by the following summation

$$\frac{1}{K_A} = \sum_i \frac{1}{k_{Ai}} = \frac{2nhL}{E}\left(\frac{1}{A_1} + \frac{1}{A_o}\right) + \frac{2h_o}{EA_o}$$

where L is the lead, n the number of leads per unit length of threaded bar, h the length of the threaded portion of the screw, and h_o the length of its non-threaded ends, A_1 the section corresponding to the outside diameter of the screw and A_o the section corresponding to its inside diameter. The last term in the expression of $(K_A)^{-1}$ assumes that L/2 is negligible compared to h_o. According to Figure 44, nh represents an exact number of leads, if it is not such a case nh will be rounded to the closest exact value.

The Torsional Stiffness Coefficient

The Torsional Stiffness of a Uniform Circular Bar

A simplified representation of an angular motion is shown in Figure 45. Assuming pure rotational spring characteristics gives

$$\Delta_T \theta = \theta_{21} = \theta_2 - \theta_1 = \frac{1}{k_T} T$$

where T is the torque of torsion applied to the bar and k_T its torsional stiffness

coefficient; k_T, in the case of a circular section, is defined by

$$k_T = \frac{\pi d^4 G}{32 \ell}$$

with d the diameter of the bar, ℓ its length and G the modulus of rigidity of its material.

The Torsional Stiffness of a Schematized Lead-Screw

Keeping the model already defined for the approximate evaluation of the axial stiffness coefficient allows the following expression for $(K_T)^{-1}$, the inverse of the torsional stiffness coefficient of the screw,

$$\frac{1}{K_T} = \sum_i \frac{1}{k_{Ti}} = \frac{16nhL}{\pi G}\left(\frac{1}{d_o^4} + \frac{1}{d_1^4}\right) + \frac{64h_o}{\pi d_o^4 G}$$

with the same notation and assumption as previously defined for the approximate calculation of the axial stiffness coefficient.

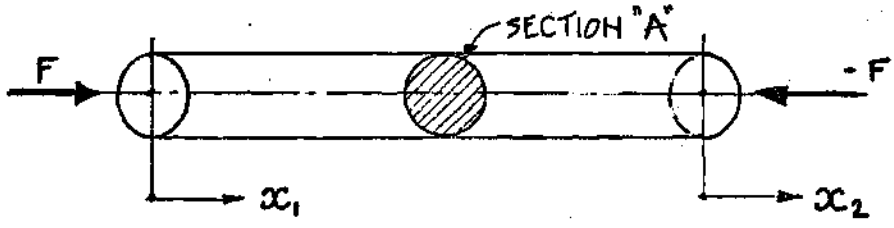

Figure 43. The Axial Stiffness of a Uniform Circular Bar.

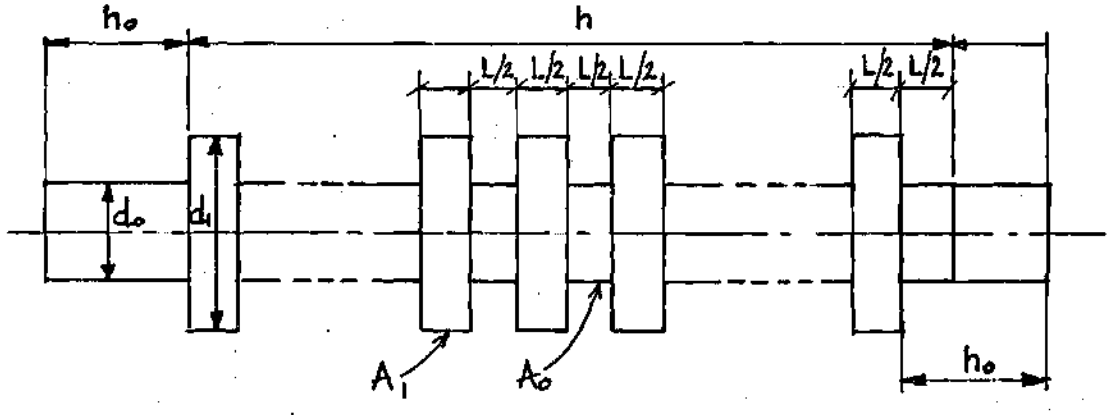

Figure 44. A Simplified Model for the Approximate Determination of the Stiffness Coefficients of a Lead-Screw.

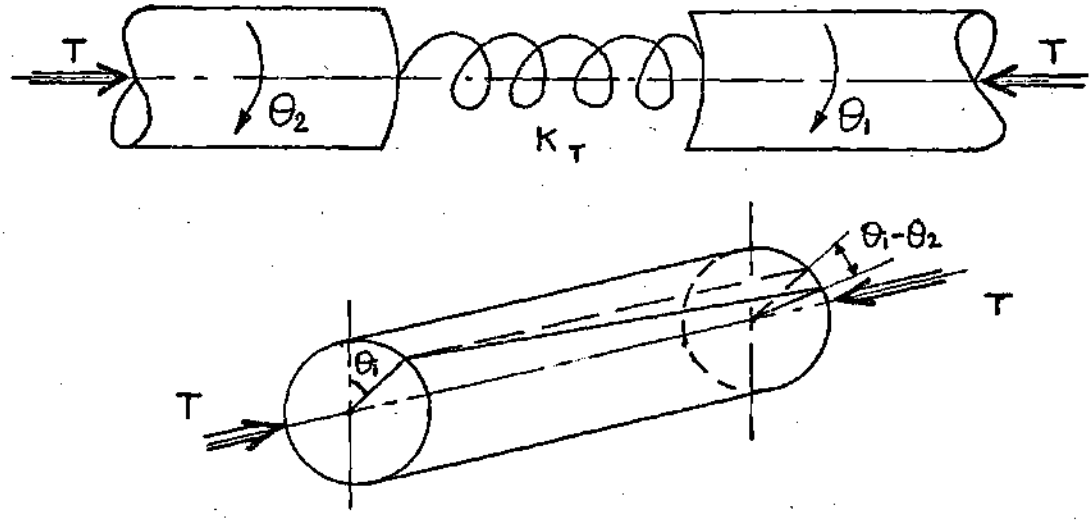

Figure 45. A Simplified Model of Angular Motion.

APPENDIX B

THE COMPLEX CONVOLUTION INTEGRAL

Let x(t) and y(t) be two time-domain functions and X(s) and Y(s) their Laplace transforms. The Laplace transform of the product x(t) · y(t) is given by

$$\left[x(t)\cdot y(t)\right] = \frac{1}{2\pi j}\int_{c-j\infty}^{c+j\infty} X(\omega)\cdot Y(s-\omega)\,d\omega$$

APPENDIX C

THE QUARTER SQUARE MULTIPLIER

Let x(t) and y(t) be two time-domain functions, their product can be simulated on an analog computer using a Quarter Square Multiplier, or Q.S.M.; this element is defined in Figures 46 and 47.

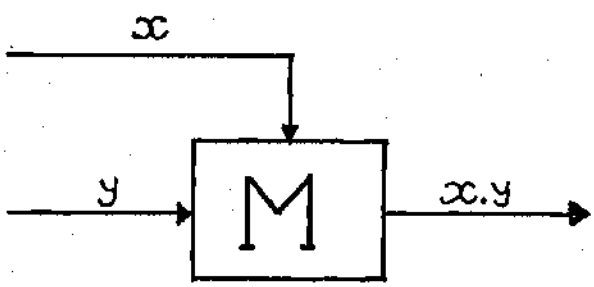

Figure 46. Symbol.

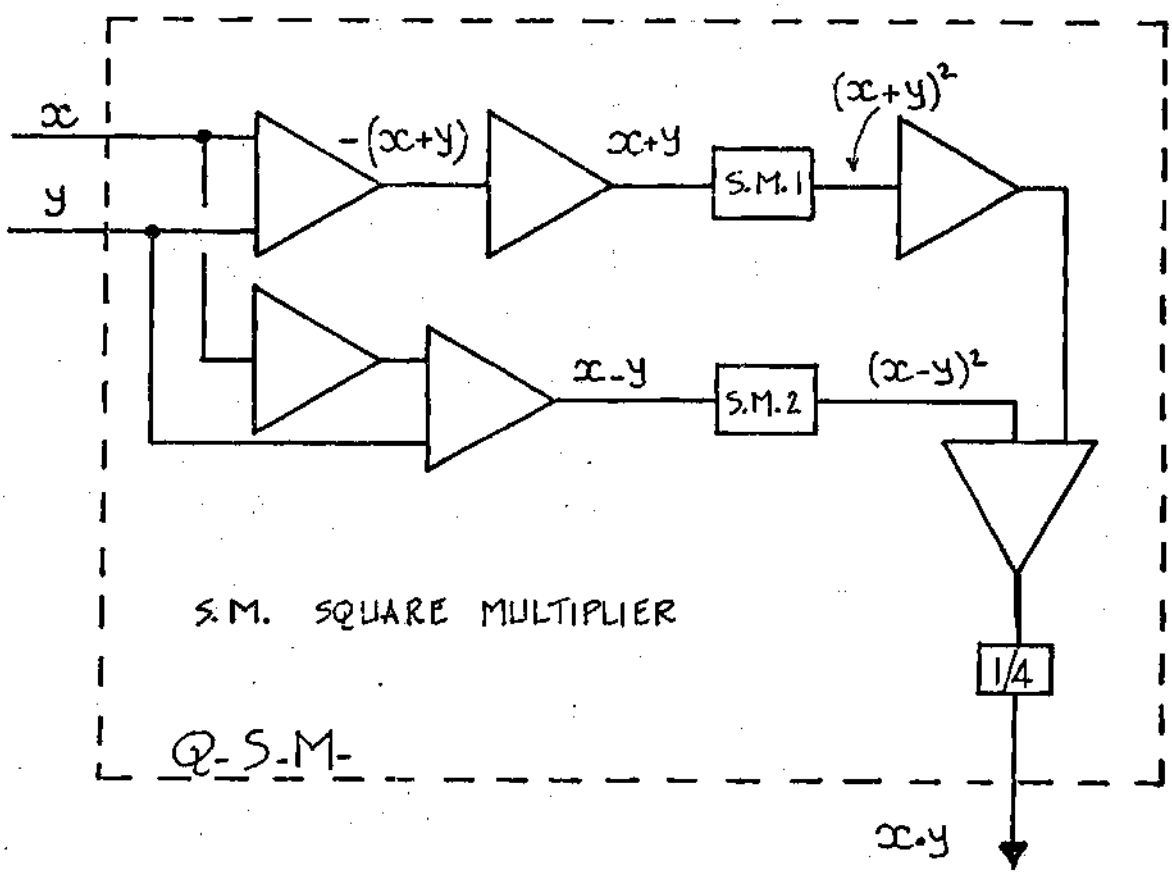

Figure 47. Computer Setup for the Quarter-Square Multiplier.

APPENDIX D

THE COMPENSATION PRINCIPLE

Notation used in Figure 48 has already been defined in Figure 35.

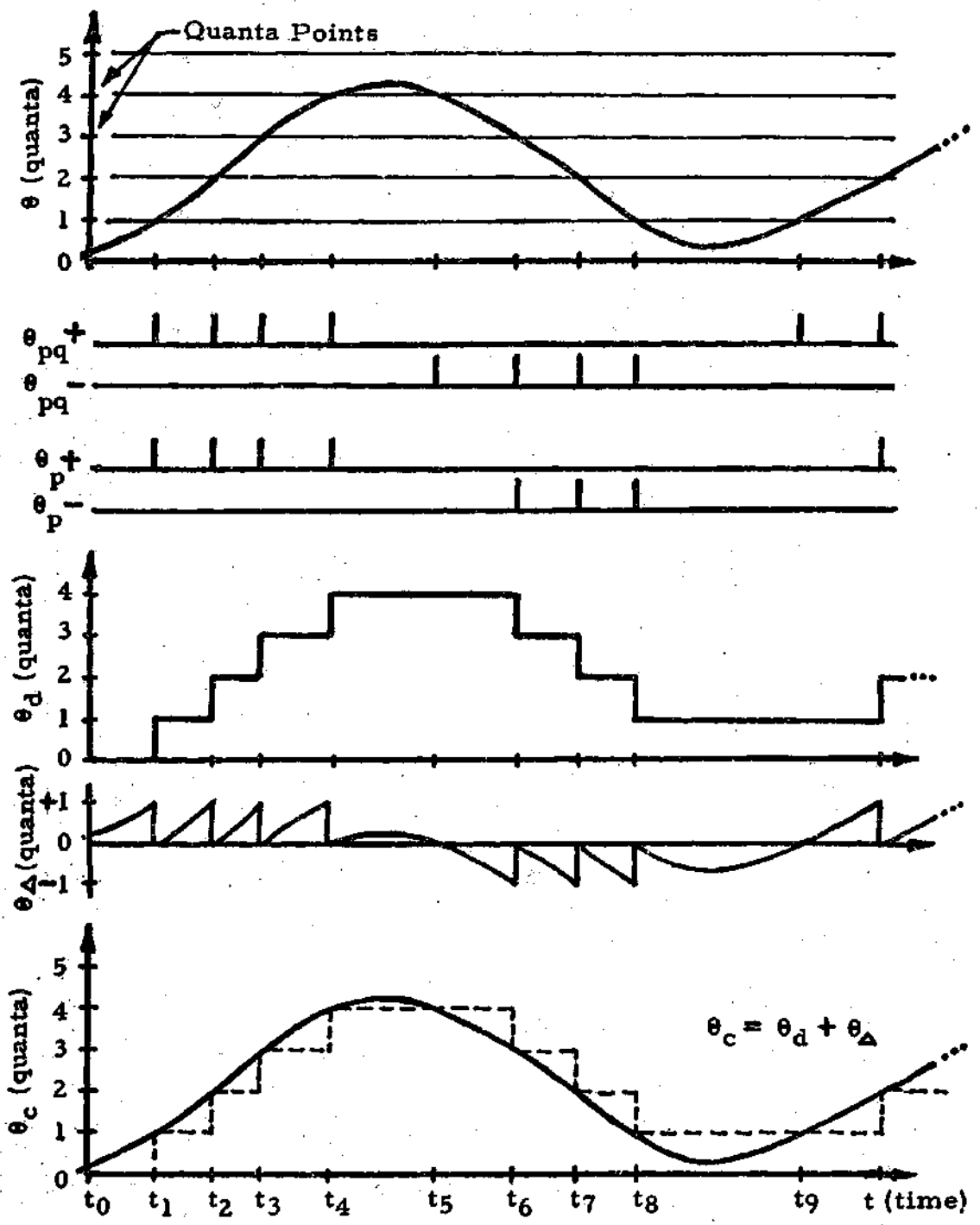

Figure 48. The Compensation Principle.

BIBLIOGRAPHY

1. J. T. Gavin, "The Machine Tool: A Multiloop Control Problem," Control Engineering, Oct. 1967.

2. J. J. D'Azzo and C. H. Houpis, Feedback Control System Analysis and Synthesis, McGraw Hill Book Company, New York, 1966.

3 Y. Takahashi, M. J. Rabins and D. M. Auslander, Control and Dynamic Systems, Addison-Wesley Publishing Company, Reading, Massachusetts, 1970.

4. J. T. Evans and L.U.C. Kelling, "Inside the Mark Century Numerical Controls," Control Engineering, May 1963.

5. H. E. Merrit, Hydraulic Control Systems, John Wiley & Sons, Inc., New York, 1967.

6. B. C. Cuppan and J. G. Bollinger, "Simulation of a Machine Tool Drive and Structure on an Analog Computer," Advances in M.T.D.R., 1966, Pergamon Press, London, 1967.

7. S. A. Tobias and F. Koenigsberger, Advances in M.T.D.R., 1965, 1966, 1967, 1968, Pergamon Press, London.

8. Z. Murase, "The Influence of the Shape and Dimensions of the Thread Form of the Ball Screw and its Break-Away Torque," Advances in M.T.D.R., 1967, Part 2, Pergamon Press, London, 1968.

9. D. A. Galonska, "Design Guide, Ball-Bearing Screws," Machine Design, Oct. 1955.

10. M. Polacek and Z. Vavra, "The Influence of Different Types of Guideways on the Static and Dynamic Behaviour of Feed Drives," Advances in M.T.D.R., 1967, Part 2, Pergamon Press, London, 1968.

11. M. Actis Dato, "Methodi Matematici per la Determinazione delle Funzioni di Trasferimento," Tesi di Laurea, 1969, Politecnico di Torino, Italy.

12. J. C. Gille, M. J. Pelegrin, P. Decaulne, Feedback Control Systems, Analysis, Synthesis and Design, McGraw Hill Book Company, New York, 1959.

13. G.A.T. Burdett, Automatic Control Handbook , George Newnes Ltd., London, 1962.

14. H. E. Merrit, Hydraulic Control Systems, pp. 133-145.

15. A. L. Holliman, Digital Control Compensation to Obtain Continuous-System Operation, PhD. Thesis, Case Institute of Technology, 1965.

16. J. J. D'Azzo and C. H. Houpis, Feedback System Analysis and Synthesis, p. 204.

17. H. E. Merrit and R. E Hohn, "Chatter, Another Control Problem," Control Engineering, Dec. 1967.

18. J. Tou and P. M. Schultheiss, "Static and Sliding Friction in Feedback Systems," Journal of Applied Physics, Vol. 24, No. 9, Sept. 1953.

19. H. E. Merrit, Hydraulic Control Systems, p.p. 294-310.